

RECLAMATION

Managing Water in the West

Improving Reservoir Evaporation Estimates

Research and Development Office
Science and Technology Program
Final Report ST-2012-7662-1



U.S. Department of the Interior
Bureau of Reclamation
Research and Development Office

March 2016

Mission Statements

The U.S. Department of the Interior protects America's natural resources and heritage, honors our cultures and tribal communities, and supplies the energy to power our future.

The mission of the Bureau of Reclamation is to manage, develop, and protect water and related resources in an environmentally and economically sound manner in the interest of the American public.

REPORT DOCUMENTATION PAGE

*Form Approved
OMB No. 0704-0188*

T1. REPORT DATE MONTH YEAR			T2. REPORT TYPE Research		T3. DATES COVERED	
T4. TITLE AND SUBTITLE Improving Reservoir Evaporation Estimates					5a. CONTRACT NUMBER R13AC80005	
					5b. GRANT NUMBER	
					5c. PROGRAM ELEMENT NUMBER 1541 (S&T)	
6. AUTHOR(S) Mark Spears, Justin Huntington and Subhrendu Gangpadhyay					5d. PROJECT NUMBER 7662	
					5e. TASK NUMBER	
					5f. WORK UNIT NUMBER	
7. PERFORMING ORGANIZATION NAME(S) AND ADDRESS(ES) Bureau of Reclamation; Technical Service Center; Water, Environmental and Ecosystems Division; Water Resources Planning and Operations Support Group Desert Research Institute; Reno, Nevada California Department of Water Resources; Sacramento, California					8. PERFORMING ORGANIZATION REPORT NUMBER	
9. SPONSORING / MONITORING AGENCY NAME(S) AND ADDRESS(ES) Research and Development Office U.S. Department of the Interior, Bureau of Reclamation, PO Box 25007, Denver CO 80225-0007					10. SPONSOR/MONITOR'S ACRONYM(S) R&D: Research and Development Office BOR/USBR: Bureau of Reclamation DOI: Department of the Interior	
					11. SPONSOR/MONITOR'S REPORT NUMBER(S)	
12. DISTRIBUTION / AVAILABILITY STATEMENT Final report can be downloaded from Reclamation's website: https://www.usbr.gov/research/						
13. SUPPLEMENTARY NOTES						
14. ABSTRACT (Maximum 200 words)						
15. SUBJECT TERMS						
16. SECURITY CLASSIFICATION OF:			17. LIMITATION OF ABSTRACT	18. NUMBER OF PAGES	19a. NAME OF RESPONSIBLE PERSON	
a. REPORT	b. ABSTRACT	c. THIS PAGE			19b. TELEPHONE NUMBER	
U	U	U	U	63	303-445-2125	

PEER REVIEW DOCUMENTATION

Project and Document Information

Project Name: Improving Reservoir Evaporation Estimates

WOID: Z7662

Document: ST-2012-7662-1

Document Authors: Mark Spears, Justin Huntington and Subhrendu Gangpadhyay

Document Date: March 2016

Peer Reviewer: Chris Pearson, Staff Research Hydrologist, Desert Research Institute

Review Certification

Peer Reviewer: I have reviewed the assigned items/sections(s) noted for the above document and believe them to be in accordance with the project requirements and standards of the profession.

Reviewer


(Signature)

Date reviewed

4/1/2016

Acknowledgements

The California Department of Water Resources (CaDWR) provided funding for the materials and construction of the Folsom Reservoir weather stations. Dr. Bekele Temesgen, Senior Land and Water Use Scientist, CaDWR, provided assistance and oversight with all aspects of the research.

David Eckhardt, Physical Scientist, Bureau of Reclamation, Technical Service Center, Water, Environmental and Ecosystems Division, Geographic Applications and Analysis Group, provided assistance with the remote sensing aspects of the research.

Executive Summary

Historically, evaporation from lakes and reservoirs has been estimated using pan evaporation information, which is widely known to have significant uncertainty both in magnitude and timing (Hounam, 1973; Morton, 1979). The objective of this research project was to improve Reclamation and State water operations and modeling in which reservoir evaporation is an important component.

This research relied on strong collaborations between the Bureau of Reclamation, Desert Research Institute, and California Department of Water Resources to design, construct, obtain required permits, and deploy four automated weather station buoys on four different western U.S. reservoirs. The four reservoirs chosen for weather station buoy deployment were Lahontan (NV), American Falls (ID), Folsom (CA), and Stampede (CA). The development of a project specific website to provide background, host the data, and enable users to efficiently visualize and download meteorological variables was a central focus of the project.

The project website was developed to host all meteorological and water temperature measurements, and estimates of evaporation for each buoy weather station, is called Open Water Evaporation Network (OWEN) and can be found at <http://owen.dri.edu>. The website gives project background, map overview, site details and photos of each buoy and installation processes, sensors descriptions, real-time graphs, and allows users to explore, visualize, and download input variables and evaporation results for the period of record at each reservoir. Details of the methods and results for each reservoir are currently summarized in a draft manuscript that is attached to this report. In summary, results highlighted in the manuscript indicate that surface temperature corrections are required to more accurately estimate vapor pressure of the water surface based on thermal-infrared measurements of the water surface, incoming longwave radiation, and emissivity estimates. A second manuscript is in preparation that details methods and comparisons of evaporation estimates derived from the aerodynamic bulk mass transfer approach, eddy covariance approach, and a remote sensing approach that relies on a combination of gridded weather data and space-borne surface temperature measurements. Preliminary results at Lake Mead indicate that remote sensing of evaporation is feasible, and depending on if bias correction of gridded weather data to in-situ measurements is carried out, absolute errors range between 10 to 20 percent (Huntington et al., 2016; Liebert et al., 2014). Application of the aerodynamic bulk mass transfer approach outlined in the James et al. (2016) manuscript, along with general study purpose and design have been recently presented at the American Meteorological Society Annual Conference (Huntington et al., 2013; Livneh et al., 2016), University of Colorado Reservoir Evaporation Workshop (<http://clouds.colorado.edu/home.html>) (Huntington et al., 2015), and Nevada Water Resources Association (Liebert et al., 2014). Also, this study supported project investigator J. Huntington to co-author a book chapter (Hobbins and Huntington, 2016) on open water evaporation techniques that is currently in press (Chapter 44, Handbook of Applied Hydrology, edited by V. P.

Singh, McGraw-Hill Education, New York), and acknowledges Reclamation Science and Technology program grant funding. These draft manuscripts, published abstracts, presentations, and in press book chapter and have spurred new interest in reservoir evaporation, and our project and sponsored reservoir evaporation workshop efforts were recently highlighted recently in Eos (Livneh et al., 2016) and a summary is planned for publication in Bulletin of the American Meteorological Society (BAMS) (Friedrich et al., 2016).

Continued operational monitoring at Lahontan Reservoir and new monitoring at Lake Tahoe (CA/NV) are planned for at least the next year. Our project team and collaborators are planning on submitting three draft manuscripts from this work in the next 1-3 months (James et al., 2016; Friedrich et al., 2016; Huntington et al., 2016). Funding for continued operational monitoring of buoy weather stations will be critical for long-term monitoring, robust benchmark datasets, and expansion of the OWEN network. Our team will be perusing funding from multiple agencies, including from Reclamation and local agencies. Our team welcomes Science and Technology funding recommendations for long-term funding, such as provided for Reclamation's AgriMet Network.

Contents

	<i>Page</i>
Review Certification.....	vii
Peer Review Documentation.....	viii
Acknowledgments.....	ix
Executive Summary.....	x
Objective	4
Approach and Partnerships	4
Methods.....	4
Results.....	7
Conclusions and Recommendations.....	9
References	11

Figures

	<i>Page</i>
Figure 1. Locations of buoy weather stations (Folsom, CA, Stampede, CA, Lahontan, NV, and American Falls, ID).....	5
Figure 2. Lahontan reservoir buoy weather station.....	6
Figure 3. American Falls reservoir buoy weather station.....	6
Figure 4. Folsom reservoir buoy weather station.....	7
Figure 5. Stampede reservoir buoy weather station.....	7
Figure 6. Screen shot of the Open Water Evaporation Network website that provides access and visualizations of near real-time and historical evaporation, meteorological, and water temperature data.....	8

Introduction

The U.S. Bureau of Reclamation (USBR) is responsible for managing water resources that sustain irrigation projects in the 17 Western states, and has been directed to address climate change in long-term water resources planning and management (Section 9504 of the SECURE Water Act). Meeting this directive relies on assumptions regarding historical and future water supplies, water demands, and climate. Reservoir operations and the development of new storage and water accounting strategies require estimates of evaporation. In addition, projected changes in open water evaporation under future climate scenarios are largely unknown, however, understanding the magnitude and timing of these changes is essential for long-term water resources planning in the Western U.S. Historically, evaporation from lakes and reservoirs has been estimated using pan evaporation information, which is widely known to have significant uncertainty both in magnitude and timing (Hounam, 1973; Morton, 1979). For example, it has been found that evaporation pans can over estimate lake or reservoir evaporation by 25 to 100% when compared to water or energy balance estimates of evaporation (Kohler et al., 1959; Sellers, 1965). Heat storage in reservoirs can alter both the rate and timing of evaporation depending on the volume, geometry, clarity, and the surrounding environment of the water body. For shallow water bodies, the heat storage impact on seasonal evaporation is minor, however, for deep water bodies it can be significant. For example, recent research in the area has found that the peak evaporation of Lake Tahoe is actually in September-November (Trask, 2007; Huntington and McEvoy, 2011), rather than in summer months as pan evaporation estimates would yield. Similar results have been found by Allander et al. (2009) for Walker Lake, Nevada. Furthermore, freezing conditions limit use of the pan evaporation method to less than half of the year in many basins. A much more serious problem in estimating evaporation over large open water bodies is the lack of over water climatological observations. Similarly, commonly available general circulation model (GCM) projections only summarize air temperature and precipitation, where air temperature is not representative of over water boundary layer conditions.

There are many methods available to estimate evaporation beyond the pan approach, however, most do not allow for programmatic computation and transfer of daily or weekly evaporation estimates via satellite or radio communications for operations purposes. The simple yet robust aerodynamic mass transfer approach has been proven accurate and suitable for near real time and seasonal estimation while accounting for the effects of heat storage (Hobbins and Huntington, 2016). This approach relies on basic weather information that can be easily collected over water and in an automated fashion. The key to measurement of weather variables is that they are measured directly over the water surface. In both arid and semi arid areas air temperature is lower, relative humidity is higher, and wind speed is elevated when collected over water verses land. A primary variable in estimating evaporation using this approach is the water surface temperature,

which is typically measured using a thermal infrared sensor. By simply measuring the water surface temperature, accounting for the effects of heat storage on evaporation can easily be accomplished.

Objective

The objective of this project was to develop a proof of concept reservoir meteorological network that consisted of weather station buoys, measuring all required weather variables and reservoir thermal properties to accurately estimate evaporation, while transferring these data in real time for operational purposes. Near real-time evaporation estimates could then be used directly in operations and management models, and to serve as bench mark datasets to refine monthly evaporation tables, and to evaluate other model estimates such as those derived from remote sensing and energy balance models. The ultimate project goal past proof of concept is to improve Reclamation and State water operations and modeling in which reservoir evaporation is an important component. Over water weather and evaporation estimates will also provide the ability to develop more robust methods for estimating evaporation, for example, through the use of space borne remote sensing data such as Landsat and MODIS.

Approach and Partnerships

The general approach for the project relied on strong collaborations between the Desert Research Institute (DRI), California Department of Water Resources (Cal DWR)(Bekele Temesgen), and Reclamation to design, construct, obtain required permits, and deploy four automated weather station buoys on four different western U.S. reservoirs. The four reservoirs chosen for weather station buoy deployment were Lahontan (NV), American Falls (ID), Folsom (CA), and Stampede (CA) (Figures 1-5). The development of a project specific website to provide background, host the data, and enable users to efficiently visualize and download meteorological variables was also a central focus of the project. DRI led the design, construction, and deployment of the weather station buoys, along with data analysis and post-processing, website development, and manuscript preparation of major findings. Reclamation led the permitting process, provided input into the design and construction of the buoys, helped with project management, and assisted in data post processing, analysis, website feedback, and manuscript preparation. Cal DWR co-led the permitting at Folsom reservoir, and assisting in field deployment and data post-processing of the Folsom buoy data.

Methods

Meteorological and water temperature variables were measured at each reservoir buoy at five minute time steps and transmitted to a DRI server (see <https://owen.dri.edu/site/sensors> for a full list and description of sensors) for estimation of evaporation. Primary variables measured at each buoy weather

station were air temperature, relative humidity, windspeed, net radiation, and water surface temperature. Once on the DRI server, numerous algorithms were mapped across the five minute time series to estimate evaporation using an aerodynamic bulk mass transfer approach (Quinn, 1979; Subrahmanyam, 2002; Tanny 2008; Verburg, 2010). For details of the bulk mass transfer approach and surface temperature corrections made for operational evaporation estimation at each buoy weather station, see Appendix 1.

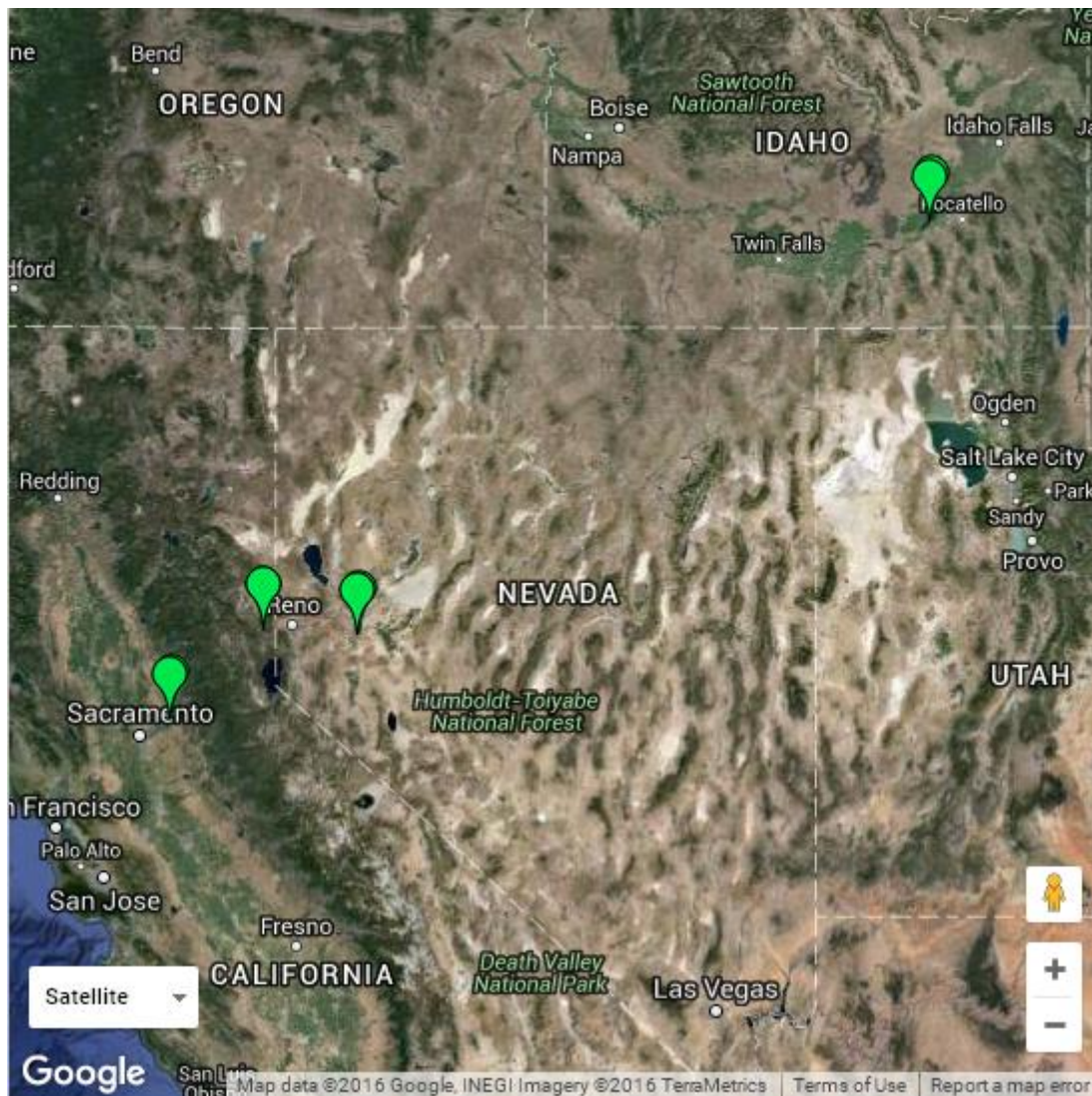


Figure 1. Locations of buoy weather stations (Folsom, CA, Stampede, CA, Lahontan, NV, and American Falls, ID).



Figure 2. Lahontan reservoir buoy weather station.



Figure 3. American Falls reservoir buoy weather station.



Figure 4. Folsom reservoir buoy weather station.

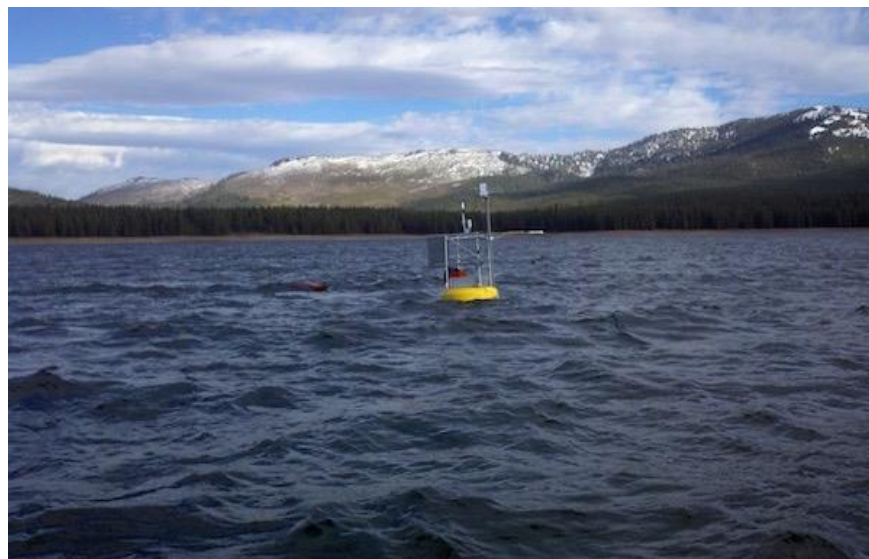


Figure 5. Stampede reservoir buoy weather station.

Results

The project website, Open Water Evaporation Network (OWEN; <http://owen.dri.edu>), was developed to host all meteorological and water temperature measurements, and estimates of evaporation for each buoy weather station. The website gives project background, map overview, site details and photos of each buoy and installation processes, sensors descriptions, real-time

graphs, and allows users to explore, visualize, and download input variables and evaporation results for the period of record at each reservoir (Figure 6).

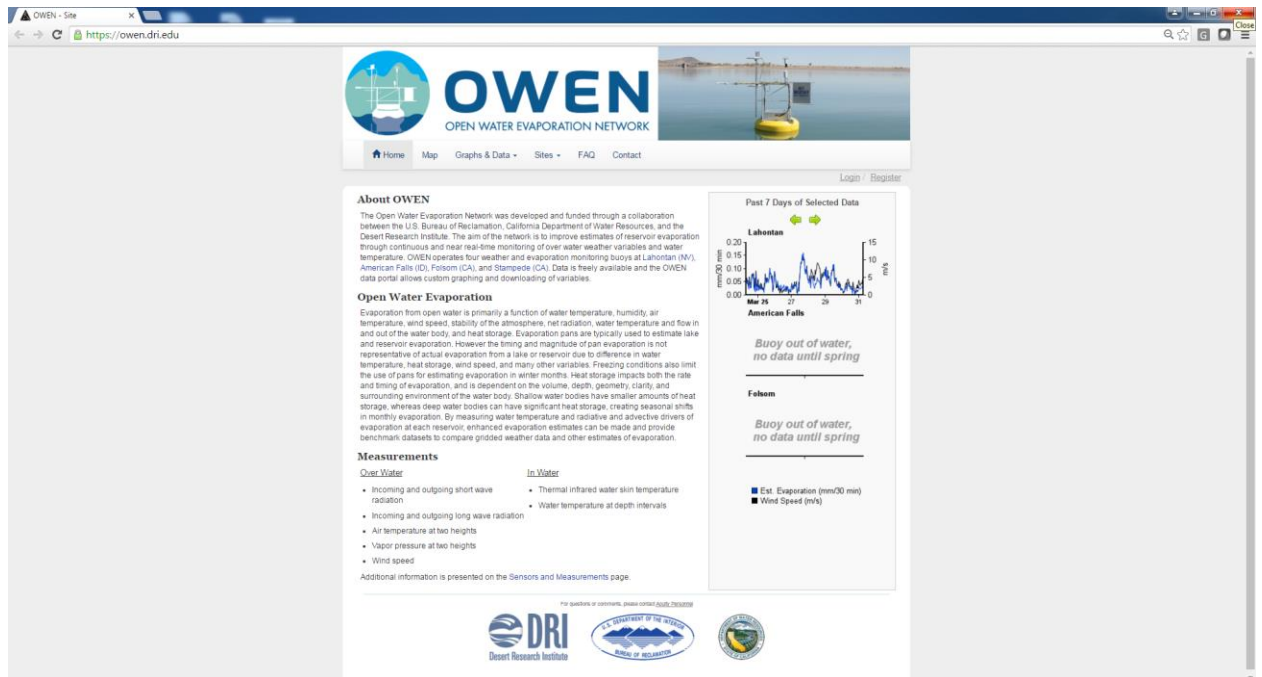


Figure 6. Screen shot of the Open Water Evaporation Network website that provides access and visualizations of near real-time and historical evaporation, meteorological, and water temperature data.

Details of the methods and results for each reservoir are currently summarized in a draft manuscript (James et al., 2016) that is attached to this report (Annex 1). In summary, result highlighted in the manuscript indicate that surface temperature corrections are required to more accurately estimate vapor pressure of the water surface based on thermal-infrared measurements of the water surface, incoming longwave radiation, and emissivity estimates. The error in estimated evaporation when using surface temperature with no correction was 7%, while the error associated with correcting for just the emissivity was significantly smaller at 4%. Results emphasize the need to apply emissivity corrections to thermal-infrared measured surface temperature when estimating open-water evaporation.

A second manuscript is in preparation that details methods and comparisons of evaporation estimates derived from the aerodynamic bulk mass transfer approach, eddy covariance approach, and a remote sensing approach that relies on a combination of gridded weather data and space-borne surface temperature measurements. Remotely sensed surface temperature is derived from Landsat and MODIS, and gridded weather data of air temperature, humidity, and windspeed is derived from hourly and daily North American Land Data Assimilation System (NLDAS) and METDATA (Mitchell, 2004; Abatzoglou, 2013). Comparisons of

in-situ, space-borne, and gridded weather data are made at bench mark study sites outlined in this report along with eddy covariance stations operated and maintained by the U.S. Geological Survey at Lake Mead and Lake Mojave (Moreo and Swancar, 2013). Preliminary results at Lake Mead indicate that remote sensing of evaporation is feasible, and depending on if bias correction of gridded weather data to in-situ measurements is carried out, absolute errors range between 10 to 20 percent (Huntington et al., 2016; Liebert et al., 2014).

Application of the aerodynamic bulk mass transfer approach outlined in the James et al. (2016) manuscript, along with general study purpose and design have been recently presented at the American Meteorological Society Annual Conference (Huntington et al., 2013; Livneh et al., 2016), University of Colorado Reservoir Evaporation Workshop (<http://clouds.colorado.edu/home.html>) (Huntington et al., 2015), and Nevada Water Resources Association (Liebert et al., 2014). Also, this study supported project investigator J. Huntington to co-author a book chapter (Hobbins and Huntington, 2016) on open water evaporation techniques that is currently in press (Chapter 44, Handbook of Applied Hydrology, edited by V. P. Singh, McGraw-Hill Education, New York), and acknowledges Reclamation Science and Technology program grant funding. These draft manuscripts, published abstracts, presentations, and in press book chapter and have spurred new interest in reservoir evaporation, and our project and sponsored reservoir evaporation workshop efforts were recently highlighted recently in Eos (Livneh et al., 2016) and a summary is planned for publication in Bulletin of the American Meteorological Society (BAMS) (Friedrich et al., 2016). Most of the published abstracts and presentations made by DRI and Reclamation study teams can be found by clicking on the hyperlinks of respective citations in the reference list.

Conclusions and Recommendations

In summary, Science and Technology grant funding that made this project possible has been extremely useful for obtaining benchmark datasets to develop and compare and contrast multiple methods for operationally estimating evaporation. DRI, Reclamation's Technical Service Center, and Cal DWR collaboration has been very successful, and we plan to continue this collaboration. In addition, continued operational monitoring at Lahontan reservoir, NV, and new monitoring at Lake Tahoe, CA/NV (pending permitting), is planned for the next 1 year based on DRI cost-share and a small amount of funding (\$39K) from re-scoping of a current Reclamation/DRI agreement. Also, this small amount of funding will be used for continued website maintenance and development. Our project team and collaborators are planning on submitting three draft manuscripts from this work in the next 1-3 months (James et al., 2016; Friedrich et al., 2016; Huntington et al., 2016). Funding for continued operational monitoring of buoy weather stations will be critical for long-term monitoring, robust benchmark datasets, and expansion of the OWEN network. Our team will be perusing

funding from multiple agencies, including from Reclamation and local agencies. Our team welcomes Science and Technology funding recommendations for long-term funding, such as provided for Reclamation's AgriMet Network.

References

- Abatzoglou, J. T., 2013: Development of gridded surface meteorological data for ecological applications and modeling. *Int. J. Climatol.*, 33, 121–131, doi:10.1002/joc.3413
- Allander, K.K., J.L. Smith, and M.K. Johnson. 2009. “Evapotranspiration in the Lower Walker River Basin, West-Central Nevada, Water Years 2005–07,” U.S. Geological Survey Scientific Investigations Report 2009-5079, 62 p
- Apogee Instruments, 2015. Emissivity Correction for Infrared Radiometer Sensors. Available online: <http://www.apogeeinstruments.com/emissivity-correction-for-infrared-radiometer-sensors/> (Accessed 2 July 2015).
- Brutsaert, W. (2005), *Hydrology: An Introduction*, 605 pp., Cambridge Univ. Press, New York.
- Brutsaert, W. (1982), *Evaporation into the Atmosphere: Theory, History, and Applications*, 299 pp., Kluwer Academic Publishers, Dordrecht, The Netherlands.
- Hobbins, M.T. and J.L. Huntington. (2015). Evapotranspiration and Evaporative Demand, Chapter 44, *Handbook of Applied Hydrology*, edited by V. P. Singh, McGraw-Hill Education, New York, in press.
<https://goo.gl/M2GNIY>
- Hounam, C.E. (1973). Comparison between pan and lake evaporation, World Meteorological Organization, Technical Note No. 126, 52p
- Huntington, J.L. and D. McEvoy, (2011). Climatological Estimates of Open Water Evaporation from Selected Truckee and Carson River Basin Water Bodies, California and Nevada. Desert Research Institute, Division of Hydrologic Sciences Publication No. 41254.
- Huntington, J.L., Mihvec, T., Allen, R., Spears, M., Rajagopal, S., Gangopadhyay, S., Eckhart, D. (2013). Development of a Reservoir Meteorological Network for Estimating Evaporation to Aid in Operations, Policies, and Procedures. American Meteorological Society Annual Meeting, Austin, TX, January 5-10.
- Huntington, J.L., Grossman, R., Friedrich, K., Blanken, P., and B. Livneh. (2015). Estimating Reservoir Evaporation Current Practice and State-of-the-Art. University of Colorado, Boulder, Reservoir Evaporation workshop, October 22-23. <https://goo.gl/Crae54>
- Huntington, J.L., Pearson, C., Morton, C., Lyles, B., Moreo, M., and R. Liebert. (2016). Remote Sensing of Open Water Evaporation using Aerodynamic-Bulk Mass Transfer Methods. *Water Resources Research*, in preparation.
- James, R., Huntington, J.L., Pearson, C., and B. Lyles. (drafted). Assessing Emissivity Effects on Estimated Evaporation using Aerodynamic-Bulk Mass Transfer Methods. Sensors.

- Kohler, M.A., Nordenson, T.J., and Baker, D.R. (1959). Evaporation Maps for the United States. U.S. Dept. of Commerce, Weather Bureau, Technical Paper #37.
- Kondo, J. 1975. Air-Sea Bulk Transfer Coefficients in Diabatic Conditions. *Boundary-Layer Meteorology* 9:91-112.
- Friedrich, K., Grossman, R., Livneh, B., Huntington, J., Blanken, P., Lenters, J., Holman, K., Finnessey, T., Kowalski, T., Healey, N., Hook, S., Prairie, J., Gochis, D., Dudhia, J., Yates, D., and K., Dahm. (2016). Reservoir evaporation: Challenges for water resource science and management in a changing world. *Bulletin of the American Meteorological Society*, in preparation. <https://goo.gl/ULACHz>
- Livneh, B., K. Friedrich, and P. D. Blanken. (2016). New interest in reservoir evaporation in western United States, *Eos*, 97, doi:10.1029/2016EO048679. Published on 23 March 2016. <https://goo.gl/3WkssE>
- Livneh, B., K. Friedrich, R. Grossman, J. Huntington, and P. Blanken. (2016). Estimating reservoir evaporation: Evaluating current and future practices and research-to-operations pathways. American Meteorological Society Annual Meeting, New Orleans, LA, January. <https://goo.gl/fjGjnm>
- Liebert, R., Huntington, J.L., and C. Morton. (2014). Estimating Open Water Evaporation for Lake Mead with Remote Sensing. Nevada Water Resources Association Annual Conference, Las Vegas, NV, February 3-6. 1st Place Student Poster. <https://goo.gl/zTsL9X>
- Mitchell, K. E., and Coauthors, 2004: The multi-institution North American Land Data Assimilation System (NLDAS): Utilizing multiple GCIP products and partners in a continental distributed hydrological modeling system. *J. Geophys. Res.*, 109, D07S90, doi:10.1029/2003JD003823.
- Moreo, M. T., and Swancar, A. (2013). Evaporation from Lake Mead, Nevada and Arizona, March 2010 through February 2012: US Geological Survey Scientific Investigations Report 2013-5229.
- Morton, F.I., (1979). Climatological estimates of lake evaporation. *Water Resources Research*, 15, 64-76.
- Quinn, F.H. 1979. An Improved Aerodynamic Evaporation Technique for Large Lakes With Application to the International Field Year for the Great Lakes. *Water Resources Research*, vol. 15, no. 4, pp. 935-940, 1979.
- Robinson, P. J., Davies, J. A. Laboratory Determinations of Water Surface Emissivity. *Journal of Applied Meteorology* **1972**, 11, 1391-1393.
- Sellers, W. D., (1965). Physical Climatology. Chicago, The University of Chicago Press, 272 pp.
- Singh, V. P., & Xu, C. Y. (1997). Evaluation and generalization of 13 mass-transfer equations for determining free water evaporation. *Hydrological Processes*, 11(3), 311-323.
- Subrahmanyam, D. B., & Ramachandran, R. (2002). Air-sea interface fluxes over the Indian Ocean during INDOEX, IFP-99. *Journal of atmospheric and solar-terrestrial physics*, 64(3), 291-305.

- Tanny, J., Cohen, S., Assouline, S., Lange, F., Grava, A., Berger, D., ... & Parlange, M. B. (2008). Evaporation from a small water reservoir: Direct measurements and estimates. *Journal of Hydrology*, 351(1), 218-229.
- Trask, J.C. 2007. Resolving Hydrologic Water Balances through Novel Error Analysis with Focus on Inter-annual and long-term Variability in the Tahoe Basin, University of California, Davis, Ph.D. Dissertation, 378 p.
- Verburg, P., & Antenucci, J. P. (2010). Persistent unstable atmospheric boundary layer enhances sensible and latent heat loss in a tropical great lake: Lake Tanganyika. *Journal of Geophysical Research: Atmospheres*, 115 (D11).

Appendix 1. Details of the aerodynamic bulk mass transfer approach (Quinn, 1979; Subrahmanyam, 2002; Tanny 2008; Verburg, 2010) applied in this report to estimate five minute and daily evaporation.

The aerodynamic method estimates vapor flux based on differential specific humidity and turbulent transfer theory where

$$E = \rho_{mair} C_E u (q_{sat} - q_2) \times t_{step} \quad (1)$$

and E is evaporation ($\text{mm } t_{step}^{-1}$), t_{step} is a time step conversion ($\text{s } t_{step}^{-1}$), ρ_{mair} is the density of moist air (kg m^{-3}), C_E is the bulk transfer coefficient, u is the windspeed at 2 m (m s^{-1}), q_2 is the specific humidity at 2 m (kg kg^{-1}), and q_{sat} is the saturated specific humidity at the water surface. C_E values for each reservoir were based on Monin-Obukhov Similarity Theory (MOST) following equations developed by Brutsaert, 1982 (see Bulk mass-transfer coefficient section below).

Measured atmospheric measurements were converted to the appropriate variables following psychrometric relationships. Saturated specific humidity at the water surface, q_{sat} , was calculated by

$$q_{sat} = \frac{0.622 e_{sat}}{P - 0.378 e_{sat}} \quad (2)$$

where e_{sat} (kPa) is the vapor pressure at the surface and P is atmospheric pressure (kPa) at the surface. Barometric pressure was not available at all sites (i.e. Stampede, CA) and was estimated from the site elevation according to the hypsometric equation when missing by

$$P = 101.3 \left(\frac{293.15 - .0065h}{293.15} \right)^{5.26} \quad (3)$$

where P (kPa) is the pressure at the given elevation and h (m) is the reservoir elevation. Vapor pressure at the surface, e_{sat} , was calculated from the water surface skin temperature by

$$e_{sat} = 0.6108e^{\frac{17.27T_{skin}}{T_{air}+237.3}} \quad (4)$$

where T_{air} is the air temperature ($^{\circ}\text{C}$), and T_{skin} is the skin temperature adjusted for both emissivity and reflected radiation ($^{\circ}\text{C}$; see Skin Temperature Correction section below). The specific humidity at 2 m, q_2 , was calculated using barometric pressure and vapor pressure

$$q_2 = \frac{0.622e_2}{P - .378e_2} \quad (5)$$

where e_2 (kPa) is the saturated vapor pressure at 2 m, found using steps similar to equations 2 and 4 above. The density of moist air, ρ_{mair} , was calculated according to (Brutsaert, 1982, 2005)

$$\rho_{mair} = \frac{P}{R_a T_{air} (1 + .61q_2)} \quad (6)$$

where P is the atmospheric pressure (Pa), R_a is the universal gas constant ($286.9 \text{ J kg}^{-1} \text{ K}^{-1}$), and T_{air} is the air temperature (K).

Bulk mass-transfer coefficient, C_E

The bulk mass-transfer coefficient, C_E , was calculated for each time-step using an iterative approach based on MOST. MOST applies stability corrections to the near surface transfer coefficients based on wind speed and atmospheric stability. The Monin-Obukhov length, L , can be used to describe atmospheric stability where, $\frac{z}{L} = 0$, $\frac{z}{L} > 0$, and $\frac{z}{L} < 0$ correspond to neutral, stable, and unstable conditions, respectively.

The iterative process relies on values of surface temperature, air temperature, wind speed, atmospheric pressure, and specific humidity. This iterative approach has been applied in various forms to estimate bulk transfer coefficients over water bodies including both oceans and reservoirs (Quinn, 1979; Croley, 1989; Tanny, 2008; Verburg, 2010; Subrahmanyam, 2002). This study follows stability functions and roughness length equations developed by Brutsaert, 1982. The general approach is presented below:

Friction velocity, u^* , can be solved by

$$u^* = \frac{u k}{\ln\left(\frac{z}{z_0}\right) - \Psi_m} \quad (7)$$

where u is average wind speed at the reference height (m s^{-1}), k is von Karman's constant (0.41), z is the measurement height (2 m in this study), z_0 is the roughness length of momentum (m) and Ψ_m is the stability function of momentum. Stability parameters Ψ_m (wind/momentum) and Ψ_v (humidity) are solved for based on atmospheric stability as follows:

Neutral Conditions ($z/L=0$)

$$\Psi_m = \Psi_v = \Psi_t = 0 \quad (8a)$$

Stable Conditions ($z/L \geq 0$)

$$\Psi_m = \Psi_v = \Psi_t = \frac{-5.2z}{L} \quad (8b)$$

Unstable Conditions ($z/L \leq 0$)

$$\Psi_m = 2 \ln\left(\frac{[1+x]}{2}\right) + \ln\left(\frac{[1+x^2]}{2}\right) - 2 \tan^{-1}(x) + \frac{\pi}{2} \quad (8c)$$

$$\Psi_v = \Psi_t = 2 \ln\left[\frac{[1+x^2]}{2}\right]$$

where $x = \left(1 - 16(z/L)\right)^{\frac{1}{4}}$.

The Monin-Obukhov length, L , can be represented by

$$L = \frac{T_v u^{*2}}{g K \theta^*}, \quad (9)$$

where T_v is the virtual temperature of the atmosphere, θ^* is the scaling temperature, g is the acceleration due to gravity (9.8 m s^{-2}). T_v can be solved by

$$T_v = T_{air}(1 + 0.61q_{air})$$

and θ^* can be solved by

$$\theta^* = [K(\theta_2 - \theta_0)] / \left[\ln\left(\frac{z}{z_{0t}}\right) - \Psi_t \right]. \quad (10)$$

The roughness length of momentum was estimated by

$$z_0 = \frac{\alpha u^{*2}}{g} + \frac{0.11\nu}{u^*} \quad (11)$$

where ν is the kinematic viscosity

$$v = \frac{4.94 \times 10^{-8} T_{air} + 1.7185 \times 10^{-5}}{\rho_{mair}}.$$

The roughness length of humidity, z_v , was estimated by

$$z_v = z_o = 7.4 \exp(-2.25(z_o u^*)^{.25}) \quad (12)$$

The above system of equations can be solved iteratively starting with equations 11, 12, and 10 using the initial conditions of $u^*=0.1 \text{ m s}^{-1}$, and Ψ_m and $\Psi_v = 0$. The iteration then continues solving equations 9, 8, 10, 11, 12, and 7 until the values converge. The final values are used to solve for C_E by

$$C_E = \frac{k^2}{\left[\ln\left(\frac{z}{z_o}\right) - \Psi_m \right] \left[\ln\left(\frac{z}{z_v}\right) - \Psi_v \right]}.$$

This final C_E value can be used in equation 1 to solve for evaporation.

Skin Temperature Correction

Following the approach for correcting skin temperature given by Apogee Instruments (2015), the longwave radiation measured by the Infrared Temperature (IRT) sensor can be expressed as

$$LW_{sensor} = \varepsilon LW_{water} + (1 - \varepsilon) LW_{in} \quad (13)$$

where LW_{sensor} (W m^{-2}) is the outgoing longwave radiation measured by the sensor, LW_{water} (W m^{-2}) is the outgoing longwave radiation emitted by the water, and LW_{in} (W m^{-2}) is the incoming longwave radiation. Equation 13 can then be reduced using the Stephan-Boltzman equation to the form

$$\sigma T_{uncorr}^4 = \varepsilon \sigma T_{corr}^4 + (1 - \varepsilon) \sigma T_{sky}^4 \quad (14)$$

where T_{uncorr} (K) is the uncorrected skin temperature reading from the sensor, T_{corr} (K) is the corrected skin temperature, T_{sky} (K) is the background sky temperature, ε is the emissivity of the water, and σ is the Stephan-Boltzmann constant, $5.670 \times 10^{-8} \frac{\text{W}}{\text{m}^2} \text{K}^4$. In this study, the IRT was positioned at approximately 45° to the normal, therefore an emissivity of 0.97 was assumed based on findings by Robinson and Davies (1972). The corrected skin temperature can be found by rearranging equation 14 to

$$T_{corr} = \sqrt[4]{\frac{T_{uncorr}^4 - (1 - \varepsilon) T_{sky}^4}{\varepsilon}}. \quad (15)$$

Using the Stephan-Boltzman equation, the background temperature of the sky can be expressed as

$$LW_{in} = \sigma T_{sky}^4 \quad (16)$$

where LW_{in} (W m^{-2}) is the incoming longwave radiation measured with the upward facing sensors of the CNR4 pyrgeometer. Equation 16 can be rearranged to estimate T_{sky}^4 as

$$T_{sky}^4 = \frac{LW_{in}}{\sigma}. \quad (17)$$

Substituting equation 17 in to equation 15 gives the corrected surface temperature that is used to estimate e_{sat} (equation 4).

$$T_{corr} = \sqrt[4]{\frac{T_{uncorr}^4 - \frac{(1-\varepsilon)LW_{in}}{\sigma}}{\varepsilon}}. \quad (18)$$

Equations 1 through 18 are executed on the DRI server every five minutes to estimate evaporation in near real-time. Five minute evaporation estimates are summed to hourly and daily timesteps for post-processing and analysis purposes.

Annex 1. James et al. (2016) manuscript in preparation for submission to Sensors.

Sensors **2015**, *15*, 1-x manuscripts; doi:10.3390/s150x0000x

OPEN ACCESS

sensors

ISSN 1424-8220

www.mdpi.com/journal/sensors

Article

Assessing Water Surface Temperature Corrections on Estimated Evaporation using Aerodynamic-

Bulk Mass Transfer Methods (Surface Temperature and Evaporation)

Riley James^{1,2}, Justin Huntington^{1,†,*}, Christopher Pearson^{1,†}, Brad Lyles^{1,†}, Mark Spears^{3,†}

¹ DRI, Division of Hydrologic Sciences, Reno, NV, USA; E-Mail: Riley.James@dri.edu (R.J.); Justin.Huntington@dri.edu (J.H.); Chris.Pearson@dri.edu (C.P.); Brad.Lyles@dri.edu (B.L.)

² Department of Physics, Occidental College, Los Angeles, CA, USA

³ United States Bureau of Reclamation; Email: jspears@usbr.gov (M.S)

† These authors contributed equally to this work.

* Author to whom correspondence should be addressed; E-Mail: Justin.Huntington@dri.edu; Tel.: +1-775-673-7670; Fax: +1-111-111-112.

Academic Editor:

Received: / Accepted: / Published:

Abstract: Daily evaporation off four reservoirs in the northwestern United States was estimated using the aerodynamic mass transfer approach. Saturated vapor pressure at the water surface was estimated from skin temperature measured by an infrared thermometer corrected for emissivity and reflected radiation, for just emissivity, and not corrected at all. Evaporation calculated using skin temperature corrected for the emissivity and reflected radiation, as well as the other values calculated using the corrected skin temperature were taken to be the correct values, and from this, the error in evaporation using the other methods was calculated to determine the importance of applying emissivity and reflected radiation corrections. The error when using skin temperature with no correction was 7.43%, while the error for correcting for just the emissivity was significantly smaller at 4.47%. Results emphasize the need to apply emissivity corrections to thermal-infrared measured skin temperatures when calculating open-water evaporation.

Keywords: emissivity; evaporation; skin temperature; water surface temperature

1. Introduction

The aerodynamic mass transfer approach is a common method for estimating open water evaporation that uses measurements of windspeed and differential humidity between the water surface and atmosphere to estimate vapor flux. This approach has shown to provide accurate operational estimates of evaporation when compared to water budget [1-3] and more data intensive and experimental methods such as eddy covariance and energy balance [4-7]. *Aerodynamic methods are simple to apply at daily time steps and require no inputs related to radiation, subsurface heat storage change, or water budget components.* Over-water vapor gradients are often estimated using saturated vapor pressure at the water surface based on skin temperature and vapor pressure of the air measured with relative humidity and temperature sensors at a defined height above the surface (e.g. 2m). In a sensitivity analysis performed by Singh and Xu (1997), the aerodynamic mass transfer method was found to be most sensitive to errors in the vapor pressure gradient. A large source of error is the water temperature used to estimate the saturation vapor pressure. This work highlights corrections and considerations for estimating surface temperature and aerodynamic mass transfer based evaporation.

Accurate measurements of water surface temperature, commonly referred to as skin temperature, are difficult to obtain with traditional temperature sensors (e.g. thermocouples) due to the small thickness of the surface layer (<1 mm), large water temperature gradients near the surface, and incident radiation and black body effects. These difficulties have led to the use of thermal infrared thermometers (IRTs) to measure skin temperature; however, standard calibration

of most IRTs does not take into account the emissivity of water or reflected incoming longwave radiation. Correcting for emissivity and reflected radiation reduces inherent sensor bias in IRT measured water surface temperatures, which in turn improves estimates of open-water evaporation by the aerodynamic mass transfer approach.

Hook et al. (2003) compared in-situ measurements of lake bulk and skin temperature with Along Track Scanning Radiometer (ASTR-2) satellite data at four monitoring stations on Lake Tahoe, NV. Using Mk I radiometers, Hook et al. (2013) estimated skin temperature by applying a correction for emissivity and reflection of incoming longwave radiation off the water to estimate the “true” skin temperature. The emissivity used for this correction was a function of wavelength and can be found in the ASTER spectral library (available online at speclib.jpl.nasa.gov). In order to find the sensitivity of various corrections, skin temperature was compared to corrections that only considered the emissivity water and not the reflection of the incoming longwave radiation off the water. They found that for skin temperatures of 5° and 20°C, not correcting for reflection of incoming longwave radiation off the water increased the estimated skin temperature by 0.200°C and 0.168°C, respectively. Similarly, Richards (1966) studied skin temperature measurements taken from aerial surveys using an IRT and found it necessary to correct for reflected longwave emissions from sky and clouds above the water in order to find the true skin temperature of the water. Results show that 0.1 to 1.5% of the radiation read by the sensor came from the reflected incoming longwave radiation. Fiebrich et al. (2003) also acknowledged slight underestimation of water skin temperature from the emissivity being less than that of a blackbody, as well as an overestimation caused by reflected longwave radiation from the target in an evaluation of measurements taken from IRT sensors.

Robinson and Davies (1972) used a spectrophotometer to estimate the emissivity of waters with varying degrees of surface contamination. Similar to previous studies, results showed a consistent emissivity of 0.97 for all freshwater

samples regardless of turbidity. In agreement, Richards (1966) found that the emissivity of water in the infrared wavelength changes with view angle, from 0.98 to 0.96 when viewed at normal and 60°, respectively.

Typical IRTs are calibrated to measure under black body conditions. To account for the lower emissivity of water, a correction must be applied based on the ratio of infrared emissions of water to that of a black body. In addition, considerations of reflected longwave radiation from the background that an object reflects when it is not a blackbody should also be considered [13]. Apogee, a manufacturer of commonly used IRTs, recommends correcting for both emissivity and reflected longwave radiation, and cautions that not accounting for these factors could result in water surface temperature errors in the range of 1 to 2°C, depending on cloud cover [14]. This study assessed the significance of emissivity and incoming radiation corrections with respect to open water evaporation estimates.

2. Methods

2.1. Data and Instrumentation

Data for this study was collected from four buoy weather stations located at American Falls (ID), Folsom (CA), Lahontan (NV), and Stampede (CA) reservoirs in the western U.S. (Figure 1). Available data collected at each site ranges from 5/2014 to 10/2014, 1/2015 to 5/2015, 3/2014 to 5/2015 and 6/2012 to 8/2014 respectively. Figure 2 shows the buoy weather station located at Folsom reservoir, CA, and is representative of the typical sensor layout at each of the other reservoirs. The buoy weather stations were designed and fabricated by the Desert Research Institute in Reno, NV with input from Reclamation and California Department of Water Resources.

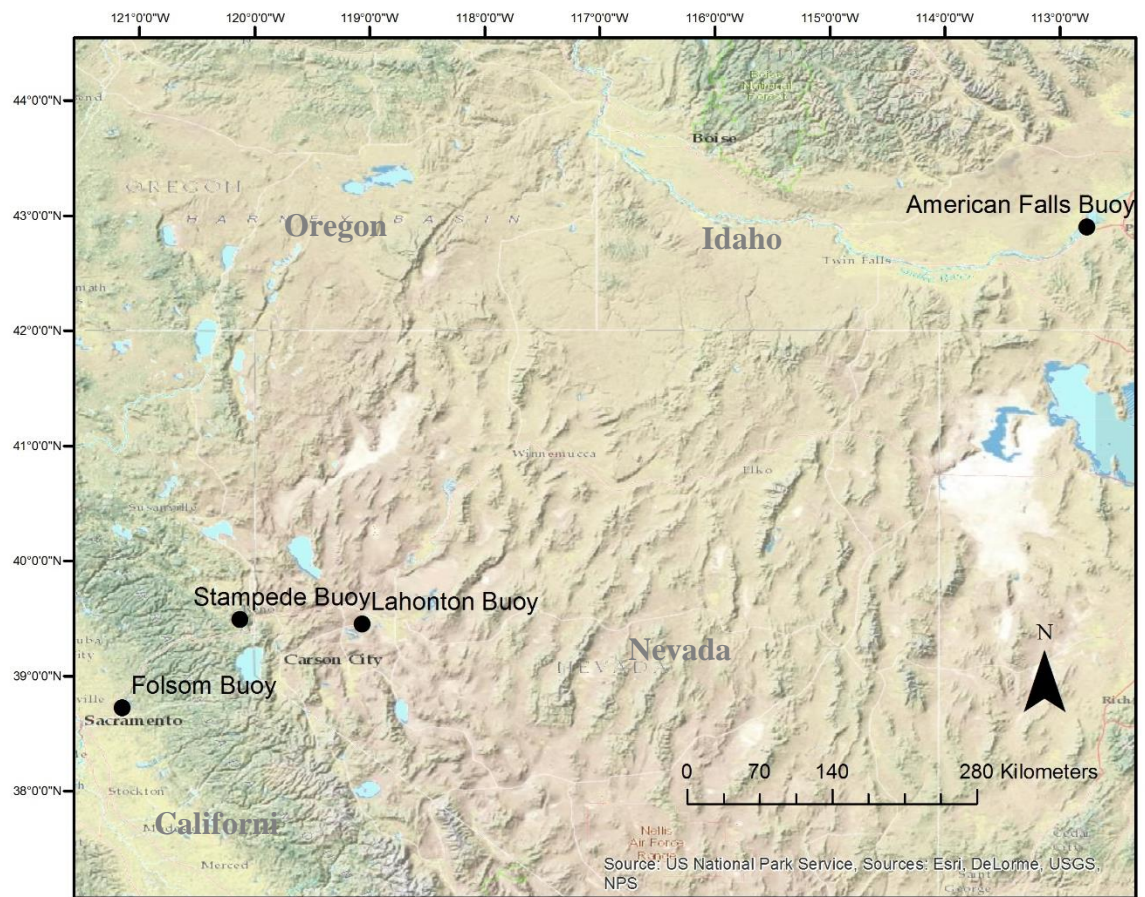


Figure 1. Locations of weather stations used to collect radiation fluxes, surface temperature, and meteorological data.



Figure 2. Buoy weather station located at Folsom reservoir, CA.

Skin temperature was measured using an Apogee SI-111 Infrared Radiometer. This sensor was chosen based on reasonable cost (under \$700) and common use for measuring surface temperature of plant canopies, soil, snow, and water surfaces. This radiometer senses radiation in the 8-14 μm wavelength range, operates in the -30 to 65 $^{\circ}\text{C}$ range, has a temperature uncertainty of 0.2 $^{\circ}\text{C}$, and is calibrated to the temperature of a blackbody cone [15]. Incoming longwave radiation was measured with a Kipp and Zonen CNR4 Net Radiometer shown on the extended arm in Figure 2. The CNR4 has a spectral range of 4.5 to 42 μm and operates in the range of -40 to 80 $^{\circ}\text{C}$ with a total daily uncertainty of under 10% [16]. Air temperature and relative humidity (RH) was measured with a Vaisala HUMICAP Humidity and Temperature Probe HMP155. The accuracy for the temperature and RH measurements are $\pm .2$ $^{\circ}\text{C}$ and $\pm 2\%$ RH, respectively, with an operating temperature range of -80 to 60 $^{\circ}\text{C}$ [17]. Barometric pressure at Lahontan, Folsom, and American Falls reservoirs was measured using an Apogee SB-100 barometric pressure sensor with a measurement uncertainty of $\pm 1.5\%$ [18]. Pressure at Stampede reservoir was estimated from the site elevation. Windspeed was measured using a R.M. Young Ultrasonic Anemometer 85106.

This device has a range of 0 to 70 m/s with an accuracy of $\pm 2\%$ from 0 to 30 m/s, and $\pm 3\%$ from 30 to 70 m/s [19]. All data was collected at 1 minute intervals and averaged to 30 minute periods.

2.2. Skin Temperature Correction

Following the approach for correcting skin temperature given by Apogee Instruments (2015), the longwave radiation measured by the IRT can be expressed as

$$LW_{sensor} = \varepsilon LW_{water} + (1 - \varepsilon)LW_{in} \quad (1)$$

where LW_{sensor} (W m^{-2}) is the outgoing longwave radiation measured by the sensor, LW_{water} (W m^{-2}) is the outgoing longwave radiation emitted by the water, and LW_{in} (W m^{-2}) is the incoming longwave radiation. Equation 1 can then be reduced using the Stephan-Boltzman equation to the form

$$\sigma T_{uncorr}^4 = \varepsilon \sigma T_{corr}^4 + (1 - \varepsilon) \sigma T_{sky}^4 \quad (2)$$

where T_{uncorr} (K) is the uncorrected skin temperature reading from the sensor, T_{corr} (K) is the corrected skin temperature, T_{sky} (K) is the background sky temperature, ε is the emissivity of the water, and σ is the Stephan-Boltzmann constant, $5.670 \times 10^{-8} \frac{\text{W}}{\text{m}^2} \text{K}^4$. In this study, the IRT was positioned at approximately 45° to the normal, therefore an emissivity of 0.97 was assumed based on findings by Robinson and Davies (1972). The corrected skin temperature can be found by rearranging equation 2 to

$$T_{corr} = \sqrt[4]{\frac{T_{uncorr}^4 - (1 - \varepsilon)T_{sky}^4}{\varepsilon}} \quad (3)$$

Using the Stephan-Boltzman equation, the background temperature of the sky can be expressed as

$$LW_{in} = \sigma T_{sky}^4 \quad (4)$$

where LW_{in} (W m^{-2}) is the incoming longwave radiation measured with the upward facing sensors of the CNR4 pyrgeometer. Equation 4 can be rearranged to estimate T_{sky}^4 as

$$T_{sky}^4 = \frac{LW_{in}}{\sigma}. \quad (5)$$

Substituting equation 5 in to equation 3 gives

$$T_{corr} = \sqrt[4]{\frac{T_{uncorr}^4 - \frac{(1-\varepsilon)LW_{in}}{\sigma}}{\varepsilon}}. \quad (6)$$

Apogee also recommends a simple correction based purely on the emissivity of water when measurements of reflected incoming longwave radiation are not available. Skin temperature using this simplified approach is estimated as

$$T_{simp} = \frac{T_{uncorr}}{\varepsilon}. \quad (7)$$

2.3. Bulk Aerodynamic Transfer Approach

This method estimates open water evaporation using the bulk aerodynamic transfer approach. This method solves for the bulk transfer coefficient, C_E , iteratively based on the Monin-Obukhov similarity equations presented in Brutsaert, 1992 ‘Evaporation into the Atmosphere’. This evaporation from this approach can be expressed for a given timestep, τ

$$E = \rho_{air} C_E u (q_{sat} - q_{air}) \times \tau \quad (8)$$

where ρ_{air} is the density of air (kg m^{-3}), C_E is the bulk transfer coefficient calculated iteratively, u is the windspeed, and q_{air} is the saturated specific humidity of the atmosphere. The saturated specific humidity at the water surface, q_{sat} (kg kg^{-1}), is given

$$q_{sat} = \frac{0.62e_{sat}}{P/10 - 0.38e_{sat}} \quad (9)$$

where e_{sat} (kPa) is the saturated water surface vapor pressure and P is atmospheric pressure (kPa) at the surface. e_{sat} is found using the equation

$$e_{sat} = 0.6108e^{\frac{17.27T_{skin}}{T_{skin}+237.3}} \quad (10)$$

where T_{skin} is the skin temperature ($^{\circ}\text{C}$) from the Apogee SI-111, adjusted for the emissivity only, or adjusted for emissivity and reflected incoming longwave radiation (i.e. T_{uncorr} , T_{simp} , T_{corr}). The saturated specific humidity of the atmosphere is given by

$$q_{air} = \frac{.62e_{air}}{P/10 - .38e_{air}} \quad (11)$$

where e_{air} is the atmospheric vapor pressure (kPa) given by the equation

$$e_{air} = \frac{RH}{100} \times .6108e^{\frac{17.27T_{air}}{T_{air}+237.3}} \quad (12)$$

where T_{air} is the temperature of the air ($^{\circ}\text{C}$) and RH is the relative humidity (%).

The bulk transfer coefficient can be found using an iterative method shown by Quinn (1979) and Crowley (1989). Under stable conditions Ce is given by

$$Ce = \frac{K^2}{\left(\log\left(\frac{z}{z_0}\right) - S_m\right)\left(\log\left(\frac{z}{z_{0q}}\right) - S_q\right)} \quad (13)$$

where K is the von Karman constant, 0.41, z is the height of the sensor (m), z_0 is the roughness length of momentum (m), z_{0q} is the roughness length of vapor (m), S_m is the stability function for momentum, and S_q is the stability function for vapor. S_m and S_q are both found using the equation

$$S_m = -.52\left(\frac{z}{L}\right) \quad (14)$$

where L is the Monin-Obhukov Length, given by

$$L = \frac{T_v u_f^2}{K g t_{fv}} \quad (15)$$

where T_v is the virtual temperature ($^{\circ}\text{C}$), u_f is the friction velocity of momentum (m s^{-1}), g is the acceleration due to gravity, $9.81 \text{ (m s}^{-2}\text{)}$, and t_{fv} is the scaling potential temperature ($^{\circ}\text{C}$). T_v is calculated using the equation

$$T_v = T_{air}(1 + .61q_{air}). \quad (16)$$

u_f is found by

$$u_f = \frac{K(u - u_f)}{\log\left(\frac{z}{z_0}\right) - S_m}. \quad (17)$$

t_{fv} is given by

$$t_{fv} = \frac{K(T_{airpot} - T_{skinpot})}{\log\left(\frac{z}{z_{0t}}\right) - S_t} \quad (18)$$

where T_{airpot} and $T_{skinpot}$ are the air and skin potential temperatures respectively (K), z_{0t} is the roughness length for temperature (m). T_{airpot} and $T_{skinpot}$ can be found

$$T_{airpot} = T_{air} \left(\frac{1000}{p}\right)^{.286} \quad (19)$$

where, when finding $T_{skinpot}$, T_{air} is replaced by T_{skin} . The roughness length for temperature and vapor are both found

$$z_{0q} = 7.4z_0 e^{-2.25\left(\frac{z_0 u_f}{\nu}\right)^{.25}} \quad (20)$$

where ν is the kinematic viscosity given by

$$\nu = \frac{4.94 \times 10^{-8} T_{air} + 1.7185 \times 10^{-5}}{\rho_{air}}. \quad (21)$$

Under unstable conditions, C_e is the same as equation 13. S_m for unstable conditions is given by

$$S_m = 2 \log\left(\frac{1+x}{2}\right) + \log\left(\frac{1+x^2}{2}\right) - 2 \arctan(x) + \frac{\pi}{2} \quad (22)$$

where x is

$$x = \left(1 - 16\left(\frac{z}{L}\right)\right)^{.25}. \quad (23)$$

S_q for unstable conditions is given by

$$S_q = 2 \log \left(\frac{1 + x^2}{2} \right). \quad (24)$$

Under neutral conditions C_e can be expressed

$$C_e = \frac{K^2}{\log \left(\frac{z}{z_0} \right) \log \left(\frac{z}{z_{0q}} \right)} \quad (25)$$

where its components are the same as both the stable and unstable conditions.

The stability is given by the Monin-Obukov Stability Parameter

$$stability = z/L \quad (26)$$

where if *stability* is greater than 0 it is stable, if it is less than 0 it is unstable, and if it is equal to 0 it is neutral. If there were more than one thirty-minute period missing in a day, that day was removed and not included in daily and monthly calculations. The percent error in estimated evaporation due to various skin temperature inputs is found by

$$Percent\ Error = \left| 1 - \frac{E_{uncorr}}{E_{corr}} \right| \times 100 \quad (27)$$

where E_{corr} and E_{uncorr} corresponds to the evaporation found using T_{corr} , and T_{uncorr} . E_{uncorr} is replaced by E_{simp} when finding the percent error for the simple temperature correction (T_{simp}). The estimated average error was weighted based on the amount of days recorded at each reservoir compared to the total number of days so that no one reservoir carried all the weight in the average error estimate across all reservoirs.

3. Results and Discussion

Figure 3 shows daily time series plots of skin temperature for each correction method. The simplified correction, T_{simp} , consistently produces the highest surface temperature estimates. This is due to the shift in emissivity from 1 to 0.97 and the unaccounted input from reflected longwave radiation. T_{corr} and T_{simp} are closest during cloud free periods when little reflected longwave radiation is present. T_{uncorr} generally produced the lowest surface temperature estimate.

Although T_{uncorr} includes additional reflected longwave radiation, the assumption of an incorrect emissivity of 1 outweighs any longwave radiation considerations. Finally, T_{corr} typically falls between T_{uncorr} and T_{simp} , but shows more variability due to its dependence on cloud cover. During periods of low incoming longwave radiation the difference between T_{uncorr} and T_{corr} is greatest, while during periods of high incoming longwave radiation, the emissivity correction is dampened and T_{uncorr} and T_{corr} will be closer.

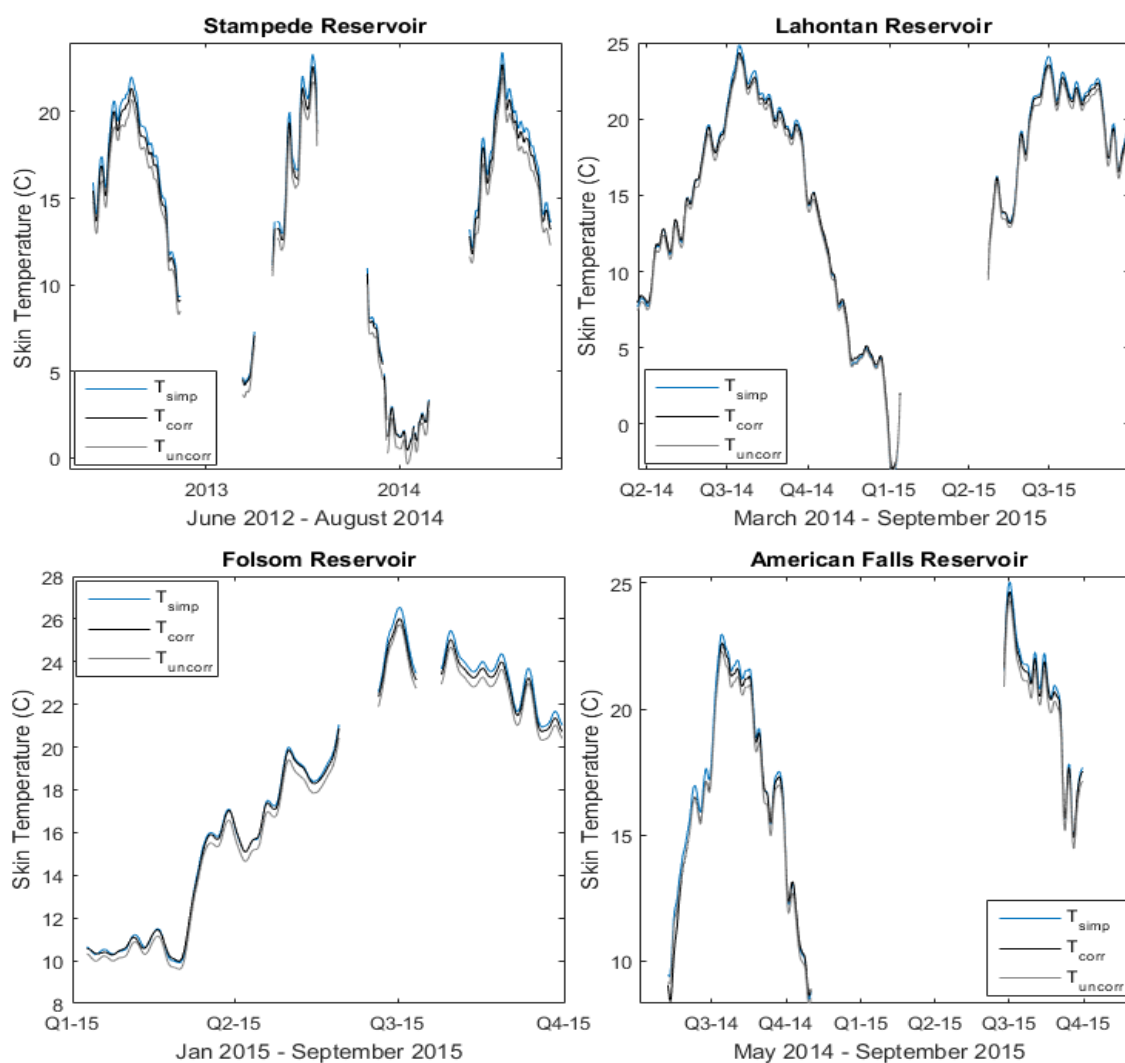


Figure 3. Skin Temperature (°C) over time. Stampede (Top Left), Lahontan (Top Right), Folsom (Bottom Left), American Falls (Bottom Right). T_{corr} (black);

T_{simple} (blue); T_{uncorr} (grey). Daily time series were smoothed for visualization purposes using a seven day moving window centered on the fourth day.

Figure 4 shows a comparison of T_{simp} and T_{uncorr} with T_{corr} at the daily time step. The T_{corr}/T_{simp} difference is generally lower than the T_{corr}/T_{uncorr} difference, except during the summer months at American Falls and Lahontan. This shift is likely caused by higher levels of incoming longwave radiation during this period (Figure 5). In agreement, the T_{corr}/T_{simp} difference is generally lowest during periods of low incoming longwave radiation. It is important to note that the seasonality of the observed patterns are very site dependent and will be a function of both outgoing long wave (i.e. surface temperature) and cloud cover.

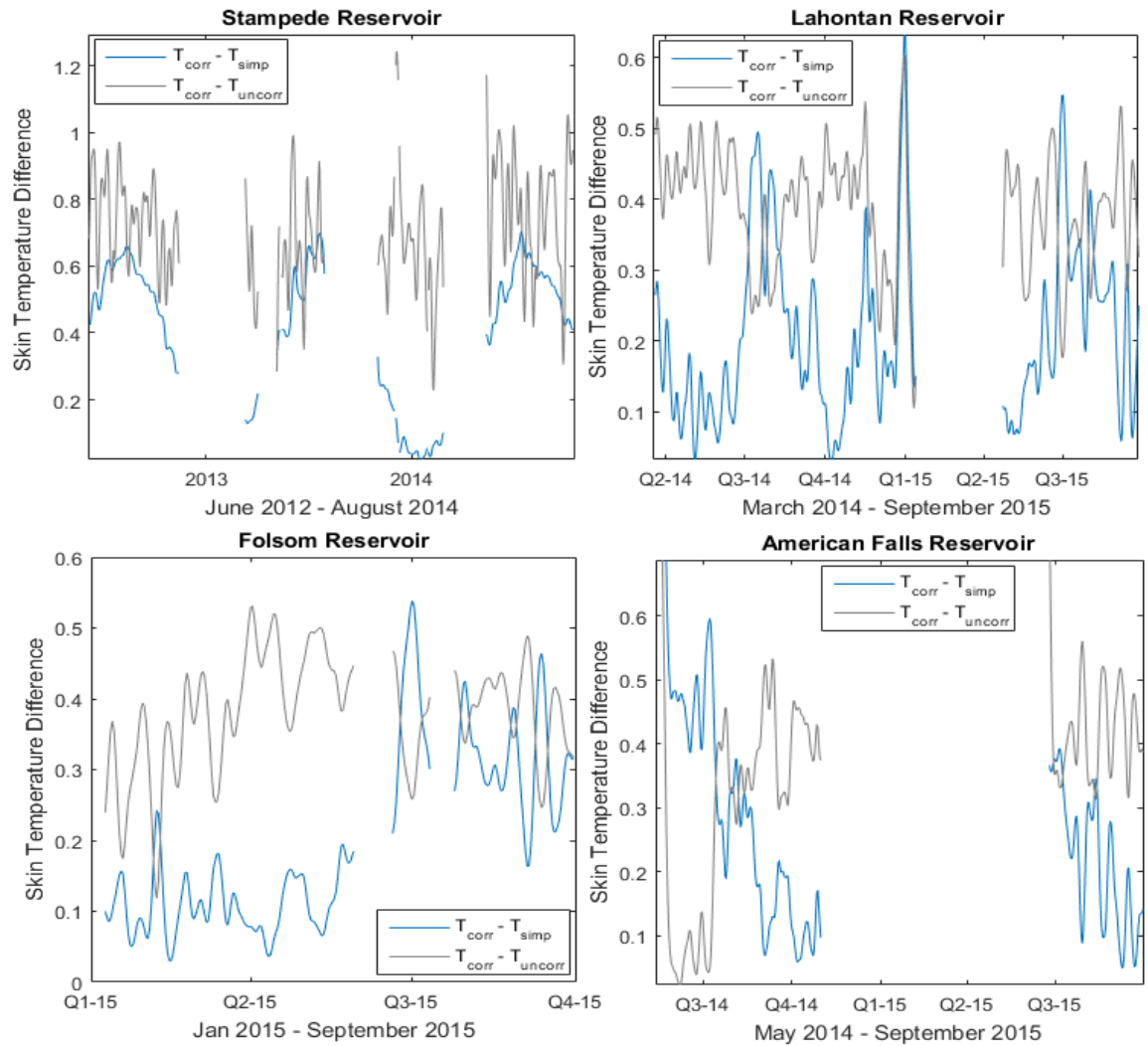


Figure 4. Skin Temperature Difference ($^{\circ}\text{C}$) over time. Stampede (Top Left), Lahontan (Top Right), Folsom (Bottom Left), American Falls (Bottom Right). $|T_{corr} - T_{simp}|$ (blue); $|T_{corr} - T_{uncorr}|$ (grey).

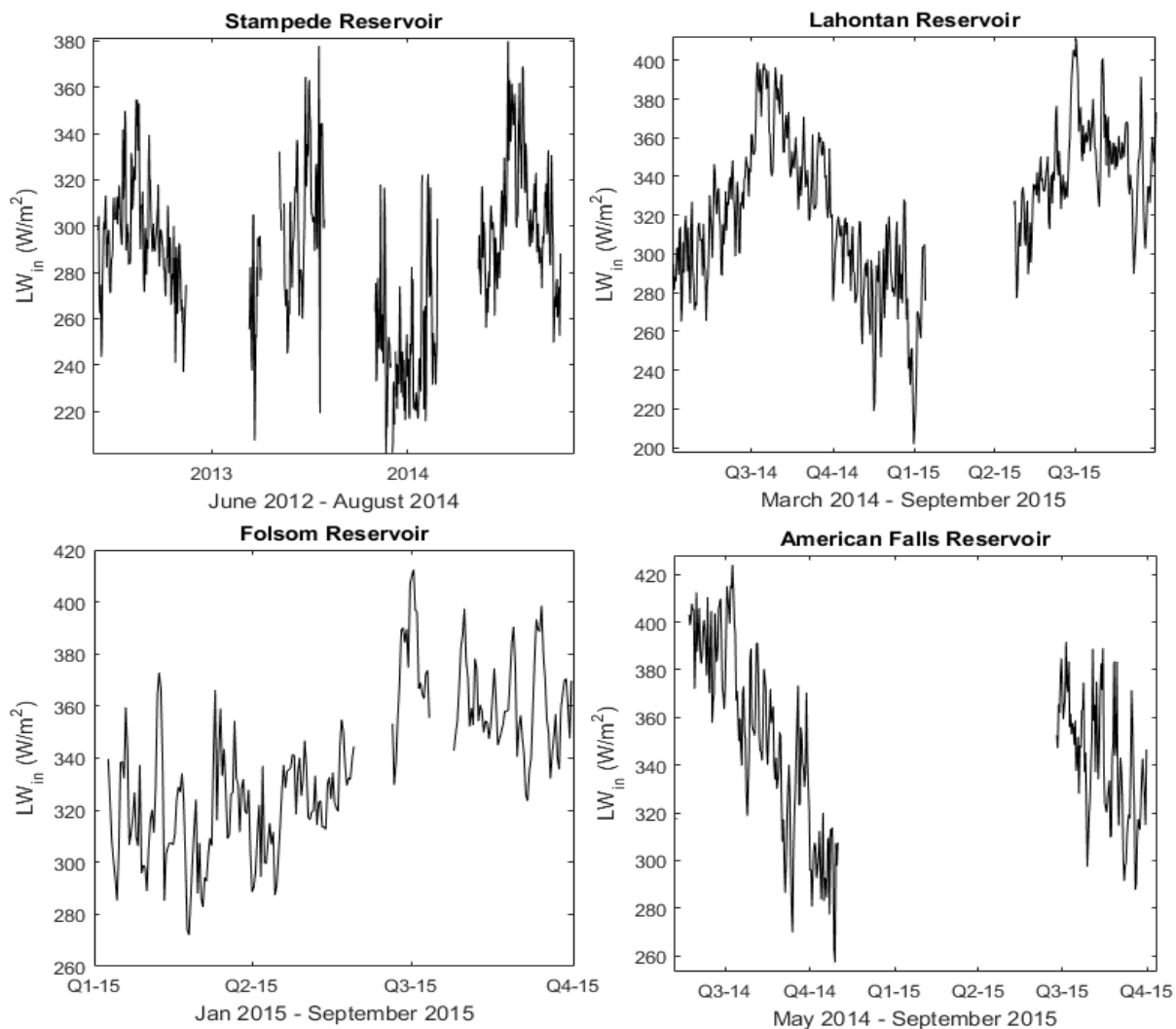


Figure 5. Incoming longwave radiation over time (W m^{-2}). Stampede (Top Left), Lahontan (Top Right), Folsom (Bottom Left), American Falls (Bottom Right).

Figure 6 shows estimates of daily evaporation based on the three different surface temperature calculations. Evaporation estimates based on T_{simp} (i.e. E_{simp})

were higher than the other two methods. The simple correction produces the highest estimates of surface temperature, which in turn yield higher saturated vapor pressure values at the water surface. These higher values produce a larger vapor gradient between the water surface and atmosphere and therefore higher overall evaporation. Similar to T_{corr} , E_{corr} estimates generally fall in between estimates of E_{simp} and E_{uncorr} ; however, during periods of low incoming longwave radiation (i.e. cloudy days), E_{corr} is closer to E_{simp} due to negligible effects from incoming longwave radiation. Similar to the skin temperature differences, the greatest difference between E_{corr} and E_{simp} occurs during mid-summer at both Stampede and Lahontan reservoirs, caused by high incoming longwave radiation during the summer months.

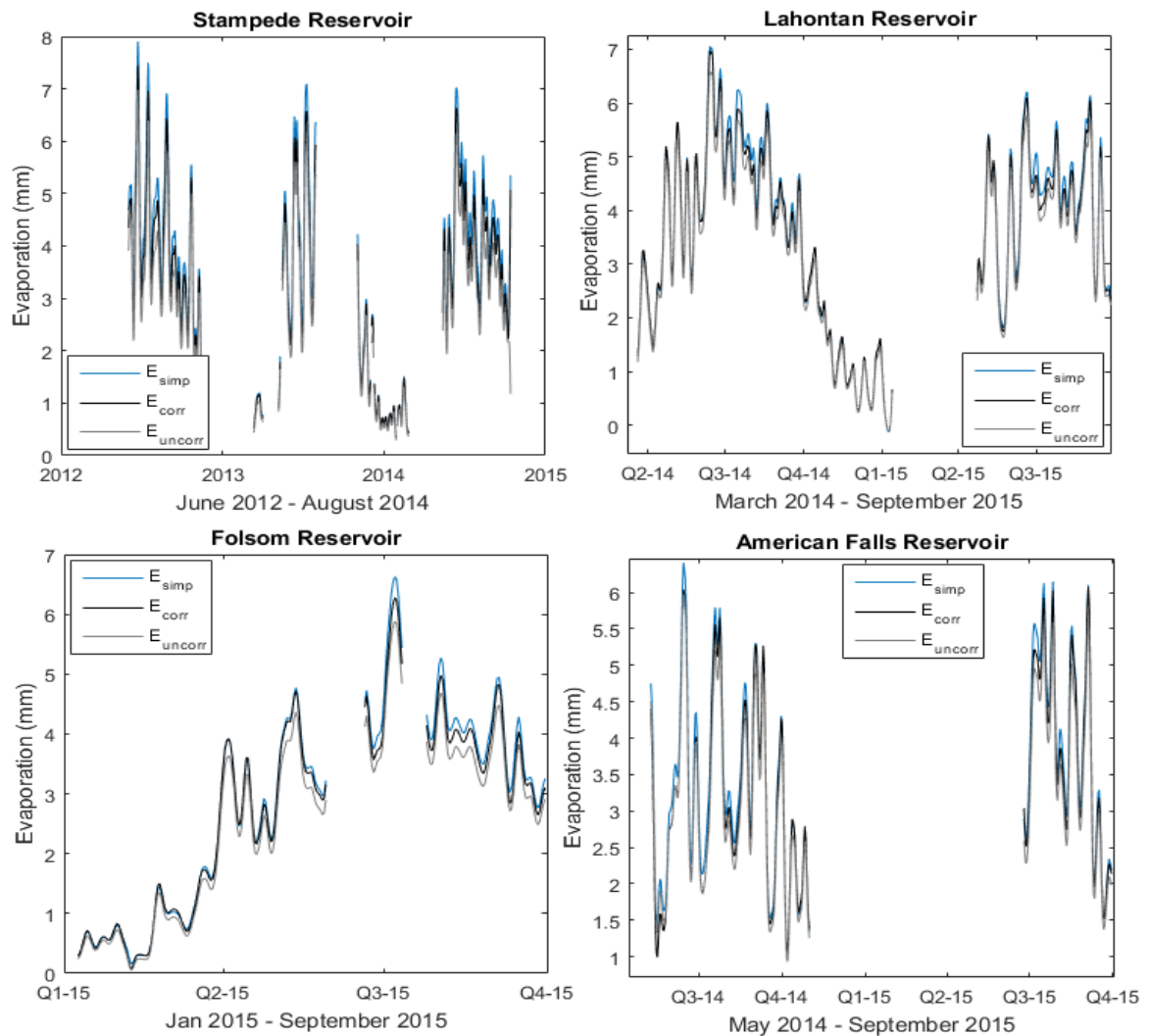


Figure 6. Evaporation (mm/day) over time. Stampede (Top Left), Lahontan (Top Right), Folsom (Bottom Left), American Falls (Bottom Right). E_{corr} (black); E_{simp} (blue); E_{uncorr} (grey). Daily time series were smoothed for visualization purposes using a seven day moving window centered on the fourth day.

To further illustrate the difference in evaporation estimates, Figure 7 shows daily ratios of E_{simp} and E_{uncorr} with respect to E_{corr} . These ratios show a lot of noise at the daily time step, but generally follow the seasonal pattern of incoming longwave radiation. The daily ratios of E_{simp} to E_{corr} are consistently higher than, and on average, closer to 1 than the daily E_{uncorr} to E_{corr} ratios. Extreme values are due to E_{corr} approaching zero as seen at Folsom reservoir in February of 2015.

The results shown in Figure 6 suggest that E_{simp} is a better estimate for E_{corr} than E_{uncorr} .

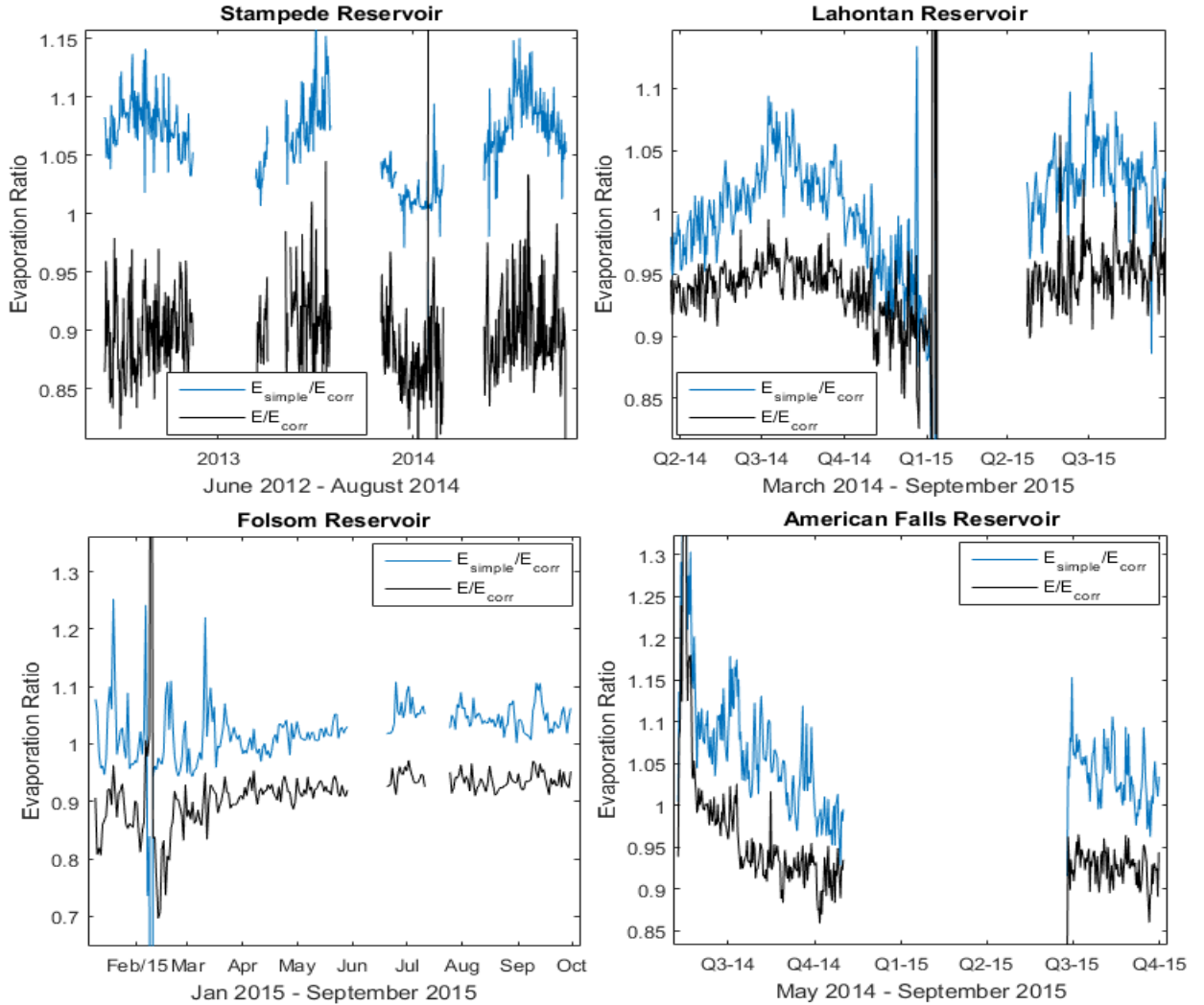


Figure 7. Daily evaporation correction ratios for the period of record for each site. Stampede (Top Left), Lahontan (Top Right), Folsom (Bottom Left), American Falls (Bottom Right). $\frac{E_{simp}}{E_{corr}}$ (blue); $\frac{E_{uncorr}}{E_{corr}}$ (grey).

Figure 8 shows 1:1 plots between daily E_{corr} and E_{simp} as well as E_{corr} and E_{uncorr} . In agreement with Figure 4, E_{simp} falls above the 1:1 line the majority of the time due to neglecting reflected longwave radiation inputs. Similarly, E_{uncorr} is

consistently below the 1:1 line due to the lack of any corrections. Occasionally, E_{simp} falls below the 1:1 line during periods when T_{simp} does not. This result is an artifact of the aerodynamic evaporation calculation relying on multiple inputs (i.e. wind speed and atmospheric vapor pressure). In addition, larger differences occur during periods of higher evaporation because saturated vapor pressure scales non-linearly with the skin temperature. This leads to greater errors in evaporation estimates during the summer and fall months when skin temperature (and evaporation) are greatest.

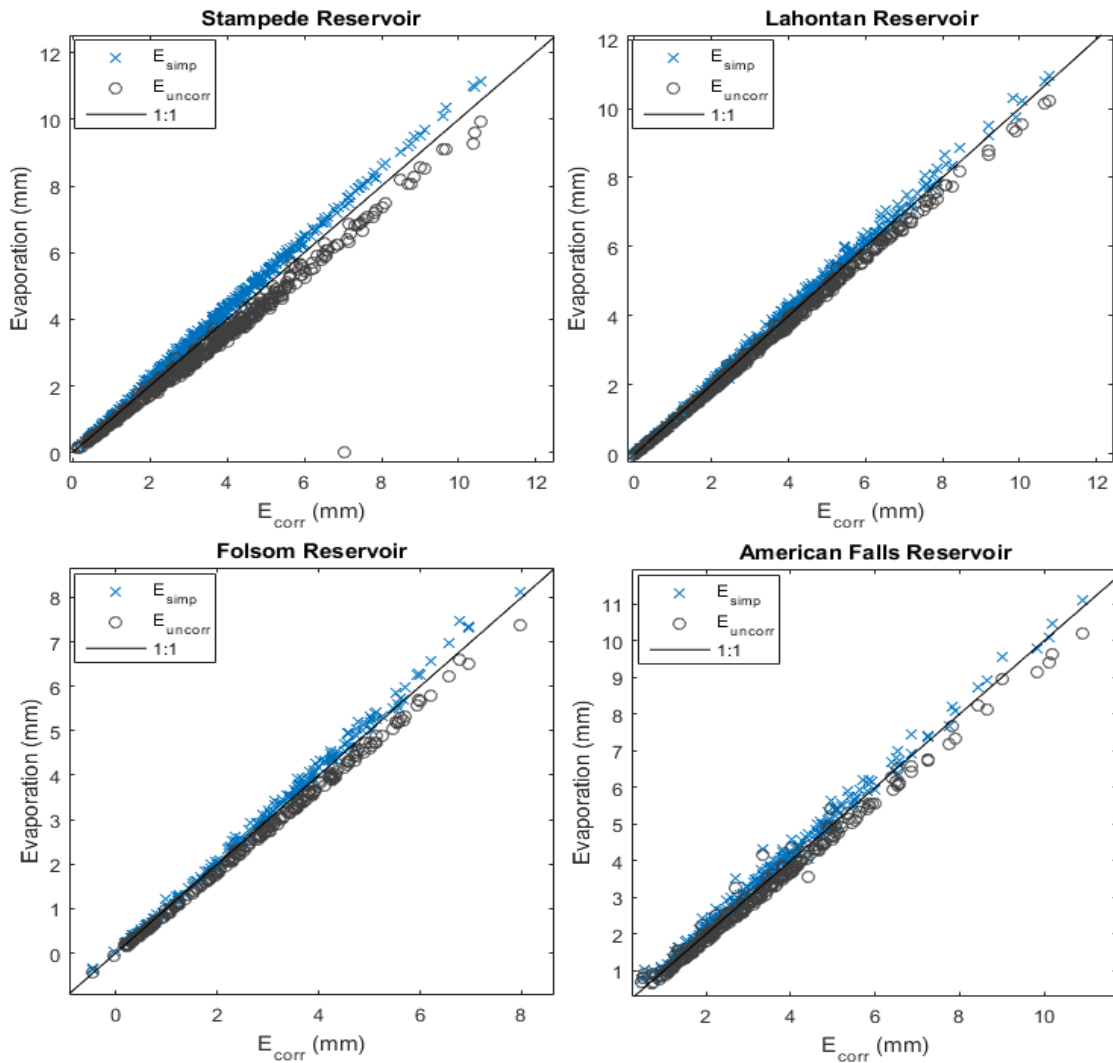


Figure 8. 1:1 plot of E_{simp} and E_{uncorr} vs. E_{corr} . Stampede (Top Left), Lahontan (Top Right), Folsom (Bottom Left), American Falls (Bottom Right). E_{simp} (blue x); E_{uncorr} (grey o); 1:1 line (black).

When incoming longwave radiation is low, so is T_{sky} . We can see from equation 6 that the smaller T_{sky} is, the less influence it has on the correction, and the closer T_{corr} gets to T_{simp} . Figure 9 shows this relationship in a 1:1 plot of T_{sky} and T_{simp} versus T_{corr} . When T_{sky} is low, T_{simp} is very close to the 1:1 line. In contrast, a larger T_{sky} causes T_{simp} to stray further from the 1:1 line.

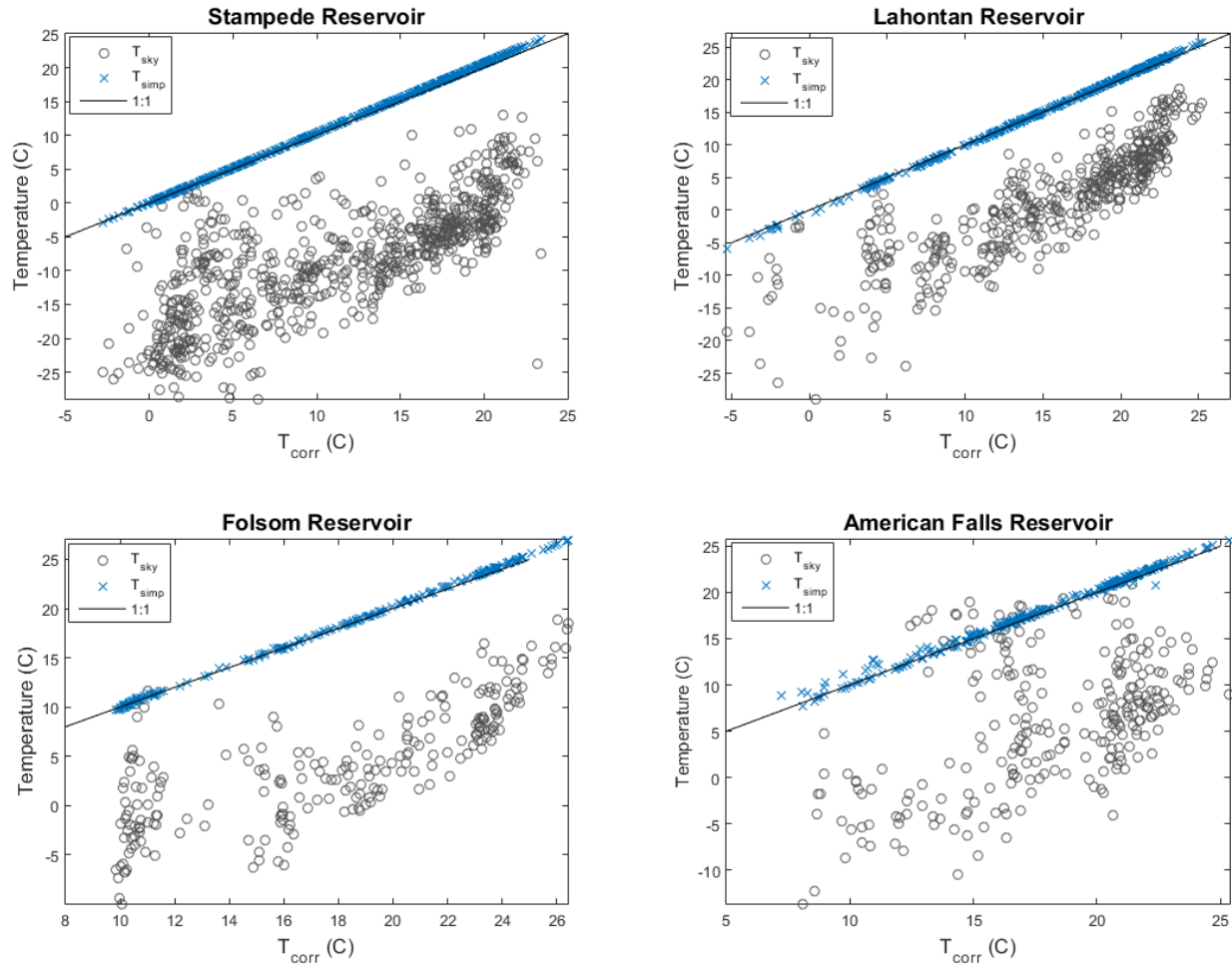


Figure 9. 1:1 plot of T_{simp} and T_{sky} vs. T_{corr} . Stampede (Top Left), Lahontan (Top Right), Folsom (Bottom Left), American Falls (Bottom Right). T_{simp} (blue x); T_{sky} (grey o); 1:1 line (black).

Monthly evaporation totals were calculated at each site to evaluate seasonality and biases in the different skin temperature corrections (Appendix Table 2). The number of days included in each total is also shown (missing days are due to sensor errors or missing data). As expected, monthly totals follow the daily estimates where E_{simp} is higher than E_{corr} and E_{uncorr} is lower.

To compare monthly totals, ratios of E_{simp} ($\frac{E_{simp}}{E_{corr}}$) and E_{uncorr} ($\frac{E_{uncorr}}{E_{corr}}$) as well as Δ_{simp} ($E_{corr} - E_{simp}$) and Δ_{uncorr} ($E_{corr} - E_{uncorr}$) were calculated (Appendix table 3). Monthly results show the error in evaporation being the highest in June, July, and August and the lowest in November, December, and January (Appendix table 3). The monthly E_{simp} ratio is consistently just above 1, with occasional dips below during the cold months at Lahontan. The ratio for E_{uncorr} is below 1 for the entire time period.

The ratio of E_{simp} to E_{corr} is closest to 1 during the winter when there is less reflected longwave radiation compared to the summer when LW_{in} tends to be higher. Conversely, the ratio of E_{uncorr} to E_{corr} is closer to 1 in the summer months and further from 1 in the winter. The overall ratios of E_{simp} to E_{corr} for the period of record at each station are 1.072, 1.018, 1.011, and 1.048, and for E_{uncorr} to E_{corr} are 0.901, 0.947, 0.913, and 0.947, for Stampede, Lahontan, Folsom, and American Falls, respectively.

Seasonal differences in the correction ratios are mainly due to differences in incoming LW radiation. Lower LW_{in} leads to lower T_{sky} , making T_{corr} closer to T_{simp} . Conversely, higher LW_{in} makes the effect of T_{sky} more significant. This relationship is clearly shown when comparing Figure 6 to the graph of Δ_{simp} in Figure 5. The two plots follow very similar paths, showing the direct influence that LW_{in} has on this difference. In contrast to T_{simp} , T_{uncorr} is closer to the T_{corr} when there is an increase in incoming longwave radiation. This corresponds to a higher T_{sky} which shifts the corrected value towards the original measurement.

LW_{in} has a seasonal dependence at each of the reservoirs, tending towards greater LW_{in} in the summer months than the winter months. This seasonality is

caused by varying cloud cover at each of the sites, which directly affect how much incoming longwave radiation is emitted. During the summer months there are less clouds, and the clouds there are usually higher and thinner, allowing for more longwave radiation to pass through, and, in the case of the thin high clouds, reflect longwave radiation from the surface. During colder months the clouds tend to be lower and thicker which let less longwave radiation through to the surface. This variation in cloud types change the amount of incoming longwave radiation, which effects T_{corr} and in turn E_{corr} [22].

The change from E_{corr} to E_{uncorr} showed monthly errors of up to 11% for the Stampede Reservoir (Appendix table 3), with an average error of 7.43% for E_{uncorr} over all reservoirs (Table 1). These errors are significant enough to affect water allocation estimates and should be taken into consideration when calculating evaporation by the aerodynamic mass transfer method. When evaluating E_{corr} with respect to E_{simp} there are monthly errors up to 17% for American Falls, with an average error of 4.79% across all reservoirs (Table 1). The errors for each individual reservoir are also much smaller for E_{simp} than for E_{uncorr} .

Table 1. Total ratios and Δ 's across all reservoirs for the period of record.

Reservoir	E_{simp} / E_{corr}	Δ_{simp} (mm)	Percent Error Simple (%)	E_{uncorr} / E_{corr}	Δ_{uncorr} (mm)	Percent Error Uncorrected (%)	Count (Days)
Stampede	1.072	-124.0	7.17	0.901	170.3	9.86	535
Lahontan	1.018	-24.9	1.82	0.947	72.0	5.26	400
Folsom	1.011	-2.9	1.11	0.913	23.0	8.66	141
American Falls	1.048	-43.8	4.79	0.947	48.1	5.25	274
Average	1.04	-65.7	4.47	0.926	101.0	7.43	338

	5						
Total	1.04	-	4.79	0.928	293.0	7.22	1350
	8	194.					
		5					

When neglecting for emissivity and reflected radiation corrections the results show significant errors that support the need to apply a correction equation to the skin temperature when available. These findings compliment the corrections made by Hook et al. (2003), Richards (1966), and Fiebrich et al. (2003) when finding the true value of the skin temperature in their studies. This also supports Apogee's claim that the error is significant when there is no correction incoming longwave radiation, and that the correction is necessary in order to determine the skin temperature accurately. As Singh and Xu (1997) pointed out, the most sensitive input variable of the aerodynamic mass transfer equation is the vapor pressure gradient, thus highlighting the need to accurately measure skin temperature for calculation of q_{sat} .

If there is no method of measuring LW_{in} or T_{sky} available, there is no way to estimate the actual T_{skin} . Because there is a lower error in estimated surface temperature when using T_{simp} , it is best to use this correction as opposed to no correction; however, it does overestimate the evaporation as opposed to the underestimation of the evaporation with no correction. The T_{simp} correction yields a surface temperature value closer to the actual temperature and is recommended when there are no LW_{in} measurements to estimate T_{corr} .

There were limitations caused by collecting data for different lengths of time at each site, causing Stampede to have the most data points and the biggest influence over the average and total values. This could cause a bias towards certain factors that do not come into play in all reservoirs. This also could affect treating the data as an overall trend for all reservoirs, instead of looking at each water body individually, such as varying cloud cover that effects incoming longwave radiation at each site. There were also gaps in the data due to a failure

in the sensors which could bias the data towards the parts of the year that data was available.

4. Conclusions

In order to assess the importance of emissivity correction in skin temperature measurements for calculating evaporation, data was taken from four reservoirs: Stampede, Lahontan, Folsom, and American Falls. Using the fully corrected skin temperature as the correct value, the ratios for evaporation were calculated to evaluate how much of an effect this correction had on the value of evaporation. Using no correction gave an average error of 7.43% across all the reservoirs for no correction, and 4.47% for the simple correction. The errors in the calculation of evaporation from non-corrected skin temperature suggest a need for emissivity and reflected radiation correction in order to make better estimates using the aerodynamic mass transfer method; however, the small errors in the simple correction provides a relatively accurate estimate when the incoming long wave radiation is not known.

Acknowledgments

Main text paragraph.

Author Contributions

For research articles with more than one author, authors are asked to prepare a short, one paragraph statement giving the individual contribution of each co-author to the reported research and writing of the paper.

Conflicts of Interest

The authors declare no conflict of interest.

Appendix

Table 2a: Evaporation totals for Stampede by month in mm (months with no data were left out of the table, signified by a line where the months are missing).

Month-Year	E_{corr} (mm)	E_{simp} (mm)	E_{uncorr} (mm)	Count (Days)
Jun-12	136.9	145.8	123.8	29
Jul-12	138.8	151.0	122.5	31
Aug-12	142.2	154.4	127.3	31
Sep-12	98.8	106.6	88.5	30
Oct-12	99.7	105.7	91.0	31
Nov-12	31.5	33.0	28.6	13
Jun-13	18.4	19.0	16.4	20
Jul-13	2.2	2.3	2.0	3
Aug-13	67.3	71.1	62.3	21
Oct-13	118.6	127.4	109.0	30
Nov-13	136.2	148.6	123.6	30
Mar-14	57.9	60.0	52.7	29
Apr-14	32.0	32.5	27.9	28
May-14	19.9	20.1	17.3	30
Jun-14	22.6	22.9	20.0	26
Sep-14	62.3	65.6	55.5	18
Oct-14	145.8	155.0	131.5	30
Nov-14	129.0	142.0	116.6	31
Dec-14	120.7	131.5	109.3	31
Jan-15	110.8	119.0	99.5	30
Feb-15	36.5	38.5	32.5	13
POR	1727.9	1851.9	1557.6	535

Table 2b: Evaporation totals for Lahontan by month in mm (months with no data were left out of the table, signified by a line where the months are missing).

Month - Year	E_{corr} (mm)	E_{simp} (mm)	E_{uncorr} (mm)	Count (Days)
Mar-14	30.2	29.5	28.3	12
Apr-14	88.3	87.0	82.9	30
May-14	129.8	129.9	122.8	31
Jun-14	161.7	164.3	153.5	30
Jul-14	161.8	170.1	155.3	31
Aug-14	143.8	148.9	136.9	31

Sep-14	115.3	117.8	109.6	30
Oct-14	73.9	73.2	68.9	31
Nov-14	35.3	33.7	32.4	30
Dec-14	25.7	24.2	23.5	31
Jan-15	2.4	2.0	2.0	13
Feb-15	23.9	23.9	22.3	8
Mar-15	105.8	107.5	100.5	31
Apr-15	135.8	139.8	129.3	30
May-15	136.3	143.3	130.0	31
Jun-15	136.9	142.0	131.5	31
Jul-15	105.8	107.8	101.1	30
POR	1370.2	1395.1	1298.2	400

Table 2c: Evaporation totals for Folsom by month in mm (months with no data were left out of the table, signified by a line where the months are missing).

Month - Year	E_{corr} (mm)	E_{simp} (mm)	E_{uncorr} (mm)	Count (Days)
Jan-15	13.2	13.2	11.6	23
Feb-15	17.3	17.4	15.0	28
Mar-15	42.7	43.1	38.4	31
Apr-15	86.9	87.2	80.1	30
May-15	105.0	107.0	96.9	29
Jun-15	43.7	45.6	41.1	11
Jul-15	89.5	95.0	84.4	18
Aug-15	123.7	129.3	115.3	31
Sep-15	104.6	109.0	98.2	30
POR	264.9	267.9	242.0	141

Table 2d: Evaporation totals for American Falls by month in mm (months with no data were left out of the table, signified by a line where the months are missing).

Month - Year	E_{corr} (mm)	E_{simp} (mm)	E_{uncorr} (mm)	Count (Days)
May-14	48.0	56.3	52.5	23
Jun-14	113.5	122.2	112.4	30
Jul-14	110.1	117.4	104.4	31
Aug-14	102.9	108.8	96.3	31
Sep-14	99.0	100.2	91.8	30
Oct-14	67.6	66.5	62.1	31

Dec-14	16.0	16.5	14.3	6
Jan-15	150.2	157.1	140.5	31
Feb-15	121.0	125.9	112.6	31
Mar-15	87.4	88.7	80.8	30
POR	915.8	959.6	867.7	274

Table 3a: Monthly evaporation ratios and Δ 's by reservoir for Stampede (months with no data were left out of the table, signified by a line where there is no data).

Month-Year	$E_{\text{simp}} / E_{\text{corr}}$	Δ_{simp} (mm)	$E_{\text{uncorr}} / E_{\text{corr}}$	Δ_{uncorr} (mm)
Jun-12	1.065	-8.9	0.905	13.1
Jul-12	1.088	-12.2	0.883	16.3
Aug-12	1.085	-12.2	0.895	15.0
Sep-12	1.079	-7.8	0.896	10.3
Oct-12	1.060	-6.0	0.913	8.7
Nov-12	1.049	-1.6	0.909	2.9
Jun-13	1.034	-0.6	0.891	2.0
Jul-13	1.058	-0.1	0.912	0.2
Aug-13	1.057	-3.8	0.925	5.1
Oct-13	1.074	-8.7	0.919	9.6
Nov-13	1.091	-12.4	0.908	12.6
Mar-14	1.035	-2.1	0.909	5.2
Apr-14	1.014	-0.4	0.871	4.1
May-14	1.010	-0.2	0.870	2.6
Jun-14	1.016	-0.4	0.886	2.6
Sep-14	1.053	-3.3	0.891	6.8
Oct-14	1.063	-9.2	0.902	14.3
Nov-14	1.101	-13.0	0.904	12.4
Dec-14	1.090	-10.8	0.906	11.4
Jan-15	1.074	-8.2	0.898	11.2
Feb-15	1.056	-2.0	0.889	4.0
POR	1.072	-124.0	0.901	170.3

Table 3b: Monthly evaporation ratios and Δ 's by reservoir for Lahontan (months with no data were left out of the table, signified by a line where there is no data).

Month-Year	$E_{\text{simp}} / E_{\text{corr}}$	Δ_{simp} (mm)	$E_{\text{uncorr}} / E_{\text{corr}}$	Δ_{uncorr} (mm)
Mar-14	0.977	0.7	0.937	1.9
Apr-14	0.985	1.3	0.939	5.4

May-14	1.000	-0.1	0.946	7.1
Jun-14	1.016	-2.6	0.949	8.3
Jul-14	1.051	-8.2	0.959	6.6
Aug-14	1.036	-5.1	0.952	6.9
Sep-14	1.022	-2.5	0.951	5.7
Oct-14	0.991	0.7	0.933	4.9
Nov-14	0.955	1.6	0.918	2.9
Dec-14	0.939	1.6	0.913	2.2
Jan-15	0.829	0.4	0.861	0.3
Feb-15	0.997	0.1	0.933	1.6
Mar-15	1.016	-1.7	0.949	5.4
Apr-15	1.029	-4.0	0.952	6.5
May-15	1.051	-7.0	0.953	6.3
Jun-15	1.037	-5.0	0.960	5.5
Jul-15	1.019	-2.0	0.955	4.8
POR	1.0182	-24.9	0.9474	72.0

Table 3c: Monthly evaporation ratios and Δ 's by reservoir for Folsom (months with no data were left out of the table, signified by a line where there is no data).

Month-Year	$E_{\text{simp}} / E_{\text{corr}}$	Δ_{simp} (mm)	$E_{\text{uncorr}} / E_{\text{corr}}$	Δ_{uncorr} (mm)
Jan-15	1.000	0.0	0.883	1.5
Feb-15	1.011	-0.2	0.870	2.2
Mar-15	1.010	-0.4	0.899	4.3
Apr-15	1.003	-0.3	0.922	6.8
May-15	1.019	-2.0	0.923	8.1
Jun-15	1.042	-1.8	0.940	2.6
Jul-15	1.061	-5.4	0.943	5.1
Aug-15	1.045	-5.6	0.932	8.4
Sep-15	1.042	-4.4	0.938	6.5
POR	1.011	-2.9	0.913	23.0

Table 3d: Monthly evaporation ratios and Δ 's by reservoir for American Falls (months with no data were left out of the table, signified by a line where there is no data).

Month-Year	$E_{\text{simp}} / E_{\text{corr}}$	Δ_{simp} (mm)	$E_{\text{uncorr}} / E_{\text{corr}}$	Δ_{uncorr} (mm)
May-14	1.173	-8.3	1.093	-4.5
Jun-14	1.077	-8.7	0.990	1.1
Jul-14	1.066	-7.3	0.948	5.7

Aug-14	1.057	-5.9	0.935	6.6
Sep-14	1.012	-1.2	0.927	7.2
Oct-14	0.984	1.1	0.919	5.5
Dec-14	1.033	-0.5	0.898	1.6
Jan-15	1.045	-6.8	0.935	9.7
Feb-15	1.040	-4.9	0.930	8.4
Mar-15	1.015	-1.3	0.924	6.6
POR	1.048	-43.8	0.947	48.1

References and Notes

1. Derecki, J. A. Operational estimates of Lake Superior evaporation based on IFYGL findings. *Water Resources Research* **1981**, *17*(5), 1453-1462. Available online: <http://onlinelibrary.wiley.com/doi/10.1029/WR017i005p01453/pdf> (Accessed on 22 July 2015).
2. Trask, J.C. Resolving Hydrologic Water Balances through Novel Error Analysis with Focus on Inter-annual and long-term Variability in the Tahoe Basin. Ph.D. Dissertation, University of California, Davis, 2007.
3. Sahoo, G. B., Schladow, S. G., & Reuter, J. E. Hydrologic budget and dynamics of a large oligotrophic lake related to hydro-meteorological inputs. *Journal of Hydrology* **2013**, *500*, 127-143. Available online: http://ac.els-cdn.com/S0022169413005416/1-s2.0-S0022169413005416-main.pdf?_tid=385a5d4c-30ac-11e5-88a3-00000aacb360&acdnat=1437595374_660814c7440828761be38db6e3cf7af3 (Accessed on 22 July 2015).
4. Harbeck, G. E., et al., Water loss investigations, Lake Mead studies, U.S. Geological Survey Professional Paper 298, **1958**. U.S. Government Printing Office, Washington, D.C.
5. Kondo, J. Air-Sea Bulk Transfer Coefficients in Diabatic Conditions. *Boundary-Layer Meteorology* **1975**, *9*, 91-112. Available online: <http://link.springer.com/article/10.1007/BF00232256> (Accessed on 15 July 2015).
6. Allen, R. G., Tasumi, M., Evaporation from American Falls Reservoir in Idaho via a Combination of Bowen Ratio and Eddy Covariance, Proceedings of the 2005 Environmental and Water Resources Institute Conference, Anchorage, Alaska, United States, May 15-19, 2015.
7. Gianniou, S. K., & Antonopoulos, V. Z. Evaporation and energy budget in Lake Vegoritis, Greece. *Journal of Hydrology* **2007**, *345*(3), 212-223.

- Available online: http://ac.els-cdn.com/S0022169407004465/1-s2.0-S0022169407004465-main.pdf?_tid=59496dea-30ac-11e5-b11b-00000aacb362&acdnat=1437595429_7a573a5d953f84112c43b8f45fb61fa8 (Accessed on 22 July 2015).
8. Singh, V. P., Xu, C. –Y. Sensitivity of Mass Transfer-Based Evaporation Equations to Errors in Daily and Monthly Input Data. *Hydrological Processes* **1997**, *11*, 1465-1473. Available online: http://folk.uio.no/chongyux/papers_SCI/HYP_2.pdf (Accessed 22 July 2015).
 9. Hook, S.J., Prata, F. J., Alley, R. E., Abtahi, A., Richards, R. C., Schladow, S. G., & Palmansson, S. O. Retrieval of Lake Bulk and Skin Temperatures Using Along-Track Scanning Radiometer (ATSR-2) Data: A Case Study Using Lake Tahoe, California. *Journal of Atmospheric and Oceanic Technology* **2003**, *20*, 534-548. Available online: [http://journals.ametsoc.org/doi/abs/10.1175/1520-0426\(2003\)20%3C534%3AROLBAS%3E2.0.CO%3B2](http://journals.ametsoc.org/doi/abs/10.1175/1520-0426(2003)20%3C534%3AROLBAS%3E2.0.CO%3B2) (Accessed on 1 July 2015).
 10. Richards, T. L. *Great Lakes Water Temperatures by Aerial Survey*. *Hydrometeorology Section, Meteorological Service of Canada* **1966**, 406-419. Available online: <http://hydrologie.org/redbooks/a070/070043.pdf> (Accessed on 8 July 2015).
 11. Fiebrich, C. A., Martinez, J. E., Brotzge, J. A., & Basara, J. B. The Oklahoma Mesonet's Skin Temperature Network. *Journal of Atmospheric and Oceanic Technology* **2003**, *20*, 1496-1504. Available online: [http://journals.ametsoc.org/doi/full/10.1175/1520-0426\(2003\)020%3C1496:TOMSTN%3E2.0.CO%3B2](http://journals.ametsoc.org/doi/full/10.1175/1520-0426(2003)020%3C1496:TOMSTN%3E2.0.CO%3B2) (Accessed on 8 July 2015).
 12. Robinson, P. J., Davies, J. A. *Laboratory Determinations of Water Surface Emissivity*. *Journal of Applied Meteorology* **1972**, *11*, 1391-1393. Available online: [http://journals.ametsoc.org/doi/abs/10.1175/1520-0450\(1972\)011%3C1391%3ALDOWSE%3E2.0.CO%3B2](http://journals.ametsoc.org/doi/abs/10.1175/1520-0450(1972)011%3C1391%3ALDOWSE%3E2.0.CO%3B2) (Accessed on July 1 2015)

13. Emissivity Correction for Infrared Radiometer Sensors. Available online:
<http://www.apogeeinstruments.com/emissivity-correction-for-infrared-radiometer-sensors/> (Accessed 2 July 2015).
14. Review of the Physics for Emissivity Correction of Infrared Temperature Measurements. Available online:
<http://www.apogeeinstruments.com/content/SI-emissivitycorrection.pdf>
(Accessed on 2 July 2015).
15. Infrared Radiometers SI-100 Series. Available online:
<http://www.apogeeinstruments.com/content/infrared-sensor-specs.pdf>
(Accessed on 9 July 2015).
16. CNR4 Net Radiometer Instruction Manual. Available online:
<http://s.campbellsci.com/documents/us/manuals/cnr4.pdf> (Accessed on 9 July 2015).
17. Vaisala HUMICAP Humidity and Temperature Probe HMP155. Available online:
http://www.vaisala.com/Vaisala%20Documents/User%20Guides%20and%20Quick%20Ref%20Guides/HMP155_User_Guide_in_English.pdf (Accessed on 9 July 2015).
18. Barometric Pressure Sensor Model SB-100. Available online:
<http://www.apogeeinstruments.com/content/SB-100manual.pdf> (Accessed on 9 July 2015).
19. Ultrasonic Anemometer Model 85106. Available online:
[http://www.nijin.com.tw/Young-Catalog/85106\(1007\).pdf](http://www.nijin.com.tw/Young-Catalog/85106(1007).pdf) (Accessed on 16 July 2015).
20. Quinn, F. An Improved Aerodynamic Evaporation Technique for Large Lakes With Application to the International Field Year for the Great Lakes. *Journal of Water Resources Research* **1979**, 15, 935-940.
21. Crowley, T. Verifiable Evaporation Modeling on the Laurentian Great Lakes. *Journal of Water Resources Research* **1989**, 25, 781-792.

22. Nasa Earth Observatory. Available online:
<http://earthobservatory.nasa.gov/Features/Clouds/> (Accessed on 27 November 2015).
23. Brutsaert, W. *Hydrology: An Introduction*, Publisher: Cambridge Univ. Press, New York, United States, 2005, pp. 605.
24. Tasumi, M. A review of evaporation research on Japanese lakes. Proceedings of the 2005 Environmental and Water Resources Institute Conference, Anchorage, Alaska, May 15-19, 2005.
25. Allen, R. G., Pereira, L. S., Raes, D., & Smith, M. Crop Evapotranspiration – Guidelines for Computing Crop Water Requirements. *FAO Irrigation and Drainage* **1998**, 56. Available Online:
<http://www.fao.org/docrep/x0490e/x0490e00.htm> (Accessed on 9 July 2015).

© 2015 by the authors; licensee MDPI, Basel, Switzerland. This article is an open access article distributed under the terms and conditions of the Creative Commons Attribution license (<http://creativecommons.org/licenses/by/4.0/>).

References

Data Sets that support the final report

If there are any data sets with your research, please note:

- Share Drive folder name and path where data are stored:
- Point of Contact name, email and phone:
- Short description of the data: (types of information, principal locations collected, general time period of collection, predominant files types, unusual file types.)
- Keywords:
- Approximate total size of all files: (folder size)